A Study of 3D Crack Patterns and Columnar Jointing in Corn Starch

by

Lucas Goehring

A thesis submitted partial fulfillment
of the requirements for the degree of
Master of Science

Department of Physics
University of Toronto

Abstract

The nature of columnar jointing has remained an enticing mystery since the basaltic columns of the Giant's Causeway in N. Ireland were first reported to science, over three hundred years ago. More recently, this phenomena, which causes shrinkage cracks to form into a quasi-hexagonal arrangement, has been shown to produce columns in a wide variety of situations and media. This report will focus on experiments investigating the nature of columnar jointing in corn starch, which has been dried using an overhead heat lamp. A study of the 3D nature of this pattern produces the first qualitative description of the ordering process, whereby a disorganized superficial crack pattern arranges itself into a quasihexagonal crack pattern at depth. Experiments probing the nature of the pattern in deep samples show that two distinct types of coarsening can increase the pattern scale. The difference between a slow, gradual shift in scale, and a sudden catastrophic jump in scale is explained by assuming that a resistance to scale change is inherent to this pattern. Such a hysteretic pattern may answer a fundamental question of columnar jointing – why the columns are so regular in the direction of their growth. This theory may be tested in other media, notably in a number of suggested measurements on basaltic colonnades. Computer control over the evaporation rate in a growing sample continues to be worked on, as do experiments revealing the dynamics of this pattern in an actively drying starch sample.

Acknowledgements

I would like to acknowledge the support and advice of my partner and parents, Eric Bond, Brian Goehring and Myrna Ziola, whose respective expertise in power electronics, geography, and graphic design were well appreciated. I thank Brian for proofreading this document. I also thank my grandmother, Frieda Ziola, who visited the Giant's Causeway with me in the spring of 2001. Fig 1.1(A-B) are her pictures from this visit.

Stephen Morris, my supervisor, gave me considerable leeway to pursue this study, both in the distribution of my time, and in laboratory resources. I thank him for his advice and for accommodating my independent style. He also contributed the images of fig. 1.1(C-E).

Lin Zhenquan was a visiting scientist from China, who worked in collaboration with me during the spring. Although the language barrier between our work was, at times, infuriating, I am thankful for his companionship and cross-cultural exchange.

My labmates have all been extraordinarily helpful, and I thank them, Zeina Khan, Anna Kiefte, Michael Rogers, Peichun (Amy) Tsai and Wayne Tokaruk, for their support.

Eduardo Jagla I thank for a continuing, and beneficial exchange of ideas. I also thank those who, in discussion, have parlayed ideas with me. These include, but are not limited to, Nigel Edwards, Mark Jellinek, Mike Marder, and Pierre-Yves Robin.

Mark Henkelman heads the MICe research center, operating out of the Sick Kids Hospital in Toronto. He graciously helped perform feasibility studies of corn starch using MRI and MicroCT, and made the center's Micro-CT services available for continued use.

Elizabeth Kates and Ester Macedo helped me translate the passages of Medieval Latin found in the earliest documents discussing columnar jointing.

Contents

List of Figures

Chapter 1

Introduction

1.1 Historical background: the story of columnar basalt

In 1693 an anonymous English nobleman, Sir R.B.S.R.S. published a brief letter in the new journal of the Philosophical Transactions of the Royal Society of London [35]. It reported his discussion with a traveller who had recently visited a natural curiosity, the Giants Causeway, in rural Ireland. This was followed almost immediately by an investigation, on the same curious geography, by Rev. Foley and Dr. Molyneux [8]. Their report included a sketch of the site, showing an unbelievable landscape composed of geometric prisms, stacked so that in cross section they tiled a great plane, running over a hundred meters from cliff edge to seashore. The columns were so closely packed that you could not fit a knife's edge between them, as shown in fig. 1.1. A nearby cliffside, locally called 'the Looms', could only be described by analogy to the long parallel pipes of a church-organ.

These philosophical gentlemen were not the first to notice strange natural columns. Molyneux cites a medieval scholar, Ansalem Boèce de Boodt, whose treatise on stones [5] describes what appears to be a basalt colonnade, and mentions an earlier author, Kentmannus [21], who writes of colonnades near Dresden. People living near such formations have often used them as natural quarries: a church near the Causeway was built of its stone [26], and an 18^{th} century scientist discovered basalt columns that had been incorporated into castle walls and city pavements in the area from Bonn to

Fig. 1.1. (A-B) Columnar jointing in basalt at the Giant's Causeway, N. Ireland. And (C-E) Devil's Postpile, California.

Cologne [44].

Around 1750, a number of similar outcroppings of columnar joints reached the attention of science [44, 36, 4], and the first tentative theory of their creation was proposed. Perhaps the columns had formed by the compression of many large boulders, originally elliptical, but squashed against each other by some great force [33]. This would explain the boundaries between columns, which would have originally been separate rocks. The flat edges of the columns would develop naturally, just like the flat surfaces found in a cluster of soap bubbles.

Over many years, attention continued to be paid to the scattered reports of natural colonnades, while consensus on the nature of their origin was long in coming. These centuries of observations have lead us to the modern understanding of how fractures form in basalt, a viewpoint which is well rooted in empirical observation. After a volcanic event, basalt pools and begins to cool. The surface quickly solidifies and fractures, while still at a temperature of 960°C [32]. The network of cracks at the surface is disordered, and resembles a mud crack pattern, favoring 90° fracture joints [32]. Such shrinkage fractures, initiated at both the top and bottom of the lava, propagate inwards, tracking the cooling fronts. At these fronts, stress is periodically relieved as cracks advance, step by step, further into the cooling rock. The crack tip leaves a record of its passage as plumose structure and striae. Plumose consists of feathery lines left in the rock – the shape of the crack tip at any instant during its growth is perpendicular to these lines [6]. The record of intermittent fracture is shown in striae, which consist of alternating smooth and rough bands on the sides of many basalts [6, 37]. The smooth bands form at the cooler edge of the rock, where the fracture starts, and where the crack tip moves fastest [37]. The rough band records how the crack tip slows to a stop as it moves into an unstrained region [37]. Water is known to seep into the cracks, stabilizing the rate at which heat is extracted from the rock [11, 3], and therefore stabilizing the penetration rate of the cooling front.

There is some qualitative evidence that the scale of this pattern is linked to the cooling rate, and that larger columns are the product of slower cooling [10, 37, 7, 23]. Often a single lava flow will contain several distinct colonnades and entablatures (disordered fracture networks) [23, 7]. Transitions between these structures are very sharp, often extending less than a meter [23, 10]. In general, a basalt flow cools

from both top and bottom. Where these cooling fronts meet, a natural discontinuity arises. Further discontinues appear between bands of colonnade and entablature, and between adjacent colonnades of different scale. The origin of these transitions, and the regularity of the columns within the separate colonnades, has remained mysterious.

In many ways, the early field researchers had a decisive lead over theoretical work. For example, a detailed survey of the Giants Causeway was made in 1879 [30]. The resulting study is still widely used, and was reanalyzed in 1983, over a century later, to discuss a novel theoretical feature – the possible evolution from a disordered surface state to a quasihexagonal crack pattern [46]. In another example, striae (see fig. 1.1), now understood to be important records of sequential fracture [6, 37], were first reported long before their modern interpretation became popular [15]. Indeed, it is only within the past 25 years that we have consistently begun to understand the shaping of these columns. Prior to this, formative ideas had been put forward involving double-diffusive processes involving chemical gradients [20], random distributions of immobile stress centers [42], or a spontaneous ordering of a horizontally bifurcating fracture [22]. These views have been superseded by the one outlined above.

But now, however, it seems this lead is being lost. Several new theoretical models, some explicitly producing a type of hexagonal crack ordering, have been proposed to explain basalt columns. Budkewitsch and Robin have proposed a maturation based on voronoi polygons [3]. Jagla and his collaborators have put forth arguments regarding energy minimization, atomistic simulation, 2D analogues, and a finite element stress analysis [17, 16, 38]. Grossenbacher and McDuffie have described a continuum thermal model [10]. These models generally agree with the existing observations coming from the study of basalt, and make predictions about the nature of this pattern. The testing of these predictions is the next logical step in this science, and was the initial incentive behind my research.

1.2 The generality of columnar jointing

There are fundamental difficulties inherent in the study of basalt. Volcanoes are difficult to control, and molten lava is not the most lab-friendly of materials. Ob-

serving the cooling of a lava lake is something that takes decades [11]. While early researchers often dissected parts of the causeway [33, 26, 8], virtually all published studies of basalt have data sets limited to two dimensional studies – either along the column faces (eg. fig. 1.1(C) or the Looms), or in cross section (such as 1.1(E) and (A) – the plain of the Giant's Causeway). It is not practical to take apart entire landscapes to study how they formed. Nor would, I think, we learn much from such a strenuous undertaking.

It has long gone unstressed, however, that columnar jointing is not unique to basalt. No, it represents a fairly general pattern that often occurs in a gradually contracting solid body. Surprisingly, many things do break into hexagons. Many igneous rocks, including mafic dykes, rhyolite, and porphyry, can fracture into columns [45, 6, 13]. Sedimentary rocks, like mud and sandstone can also be columnar [6, 40]. Septarian concretions, unusual broken ellipsoidal shales and mudstones (often concteted together with later deposits of material) [39, 34], may also be an incarnation of columnar jointing. Even metamorphic rocks, such as coal or smelter slag, have been reported to form columnar joints [6]. Simple everyday materials of glass and starch, were discovered to fracture into columns by French in 1922, but largely ignored until Müller's recent rediscovery of joints in desiccated corn starch [28, 27, 29]. One last example of columnar jointing I find particularly amazing: ice. Simple water, with the addition of a particular colloid, and flash frozen, splinters into micrometer sized pillars [25]. Combined with the largest basalt columns (several meters across), these examples span an enormous range of material properties, and display a single phenomena across six orders of magnitude of scale. Indeed, as lava is constantly being spewed from deep sea ridges, it is conceivable that the majority of the earth's surface could (although this is pure speculation) be covered with such slender columns of rock. On the moon, much of which is covered with basalt, columnar joints were noticed on the Apollo 15 mission [19]. Attempts have even been made to explain fractures in the crust of Venus via columnar jointing [18]. This is thus a very widespread, and poorly understood, phenomena.

There has been a renewed interest in fracture phenomena in physics recently. Strange and beautiful patterns have been observed to form when a solid is broken in just the right ways. Snakelike waves and spirals, as well as complex fractal forms, are

possible [2, 47, 24]. How fracture patterns form is only ambiguously understood, as is the range of material properties and situations under which certain patterns develop. So far, hexagonal fracture patterns have been largely ignored in this renaissance, but they should be no more.

1.3 A short primer on crack mechanics

Two dimensional crack patterns are relatively well understood, including some patterns that form the 2D analogue of columnar joints. In thin films, as is illustrated in fig. 1.2, the formation of random crack networks can be understood through the stress distribution [41].

Directionally dried crack patterns, including a 1D fracture front penetrating a 2D medium, offer some interesting insights into the patterns of columnar joints. When such a front is set up, the primary cracks in TiO_2 [41] and sol-gel [14] mature into a set of equally spaced parallel cracks. Jagla and Rojo have recently showed how the stress ahead of such a line of crack tips will act to even out the distance between cracks [17]. In both TiO_2 and sol-gel the spacing of the cracks increases as the medium thickness was increased. But, in TiO_2, if the thickness is suddenly changed during drying, there are conditions when the pattern scale will not adapt, implying a range of pattern scales are allowed for any given thickness [41].

Many of these observations apply to columnar joints. The scale is set by the drying conditions, and as I shall show, can be hysteretic. As the cracks grow, there are tendencies towards order and uniformity, just as there is a 2D trend to equally spaced cracks. However, the standard ideas of thin film fracture are problematic when approaching 120° joints, which cannot be explained by such a simple point of view. Also, there is the problem of finding what, fundamentally, sets the scale of the crack spacing, in both 2D and 3D patterns.

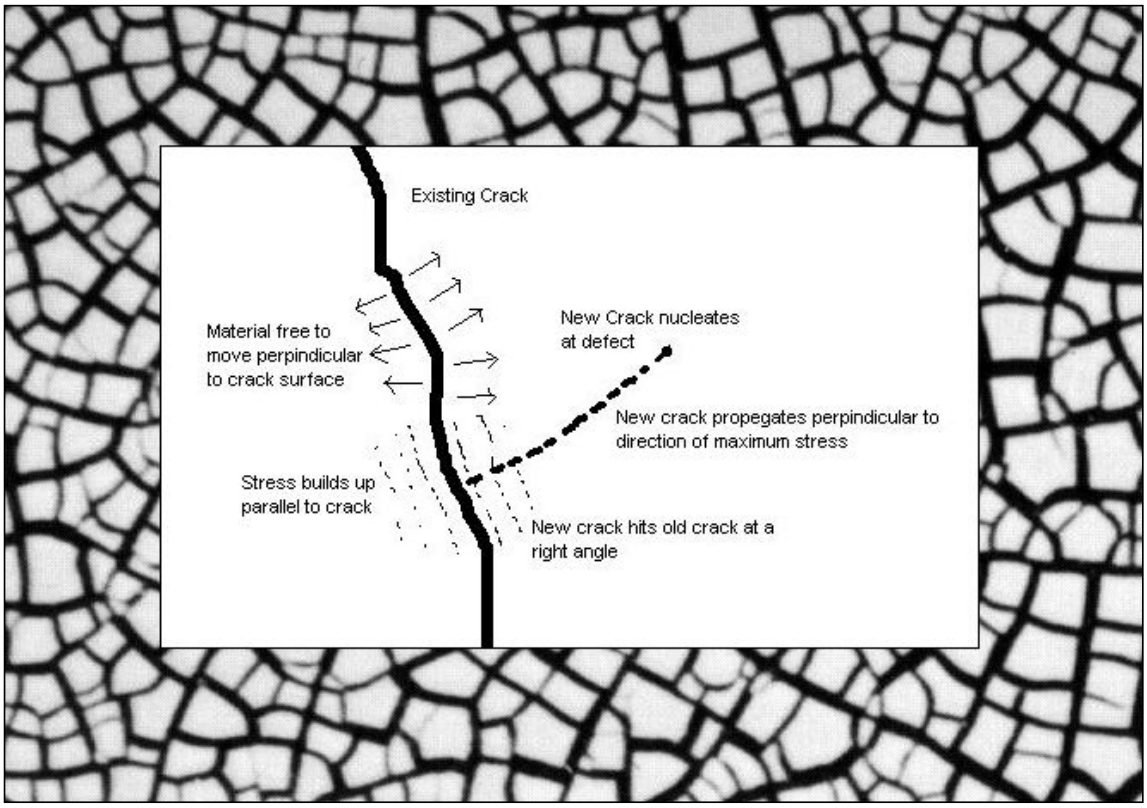

Fig. 1.2: An introduction to crack mechanics in thin films (see ref. [41]).

Consider a nearly homogeneous medium which is being uniformly dried. The drying will cause stress to build up, as the material shrinks. The stress is best described by a tensor field, and a crack tip will usually propagate in the direction of maximum stress, such as to relieve the most energy. Cracks nucleate at microscopic defects, and, if the medium is stressed enough, propagate quickly. Once a shrinkage crack has formed, the adjoining sides are free to adapt to stress by moving in a direction perpendicular to the crack. This releases some stress, but does not affect stress build-up parallel to the crack. Thus, when a new crack tip gets near this existing crack, it will bend to meet the old crack at a right angle. The background of this figure is a shrinkage pattern formed in this manner [41].

Chapter 2

Studies of columnar jointing in corn starch

2.1 Experimental techniques

In this study, columnar jointing was studied in desiccating corn starch. An initial investigation using six different types of starch (rice flour, potato flour, corn meal, corn starch, wheat flour and cake flour) showed that corn starch (100% pure, Bestfoods Canada Inc., Toronto) formed good columns, a few mm in diameter. The only other medium to form columns was potato starch. Corn starch was chosen for these studies due to the prior work done by Müller on it, and because it was found to be easier to work with than potato starch. Other early experiments involving TiO_2 and bentonite did not produce columnar joints.

My experimental techniques are based on, and extend upon, those used by Müller [28, 27, 29]. An initial water to starch ratio of 1:1 was used consistently in these experiments. Getting an evenly mixed sample was difficult with less water, while if more water is used, it simply pools at the top of the sample. To test the initial hydration of starch, 78.10 g of starch were weighed into, and spread thinly over, a tinfoil weigh boat, and placed under vacuum for 24 hours. The subsequent weight loss showed the starch reagent contained 1.9 % water, by mass. Additional water could be strongly bound to the starch, but due to the difficulty of extracting it, should not affect the experimental results. The hydration level of the starch is likely variable,

depending on the humidity of the air. Due to these considerations, and accounting for slight variations during experimental preparation, it is unlikely that we can expect better than a 5% accuracy in the water to starch ratio. Fortunately, since columnar jointing does not begin until much of this water has evaporated, the precise initial concentrations are not likely to affect these experiments.

The starch is slowly desiccated by overhead heat lamps (250W halogen bulbs). The distance between the lamp and the starch determines the evaporation rate, which could be initially varied from 10-40 mg cm^{-2} h^{-1}. The samples were dried in glass roundbottom containers, and in beakers. Depths from 1-100 mm were used. As it was found that mould grew in the starch samples after 3-4 days of drying, a few ml of bleach were added to each sample, as an antiseptic. Comparison of bleach-less and bleached samples showed no difference in the crack patterns.

Laboratory data was mostly in the form of digital photography. A Canon PowerShot S200 was used, with 2 megapixel images. Using external magnification in the form of glass lenses held by a retort stand, any structure larger than 0.1 mm large could be clearly resolved. Three methods were used to gather data on the structure of the fully dried starch plugs. A comparison of the various methods is shown in fig. 2.1.

The easiest method was to examine the counterparts left on the base of the glass containers used to grow the samples. Where the cracks meet the plate, a white ridge of starch remains attached to the plate. Also, at the center of each polygon, a dot of starch remains. These points represent the central point of the columns where no motion occurred as the cracks grew [28]. The main problems with this form of observation was that it is limited to one depth per sample, that it has poor resolution of small scale structures, and that the record is very fragile, and often incompletely formed. It is, however, simple, clean, and allows a good confirmation of the repeatability of the results.

The next technique is the direct imaging of the starch itself. This was problematic, however, in getting a good contrast between starch and crack. To enhance contrast, fine ($<75\mu$m) grains of black sand were dusted over the imaging surface, and ground into the cracks by gently rubbing the surface with a finger, while any excess was blown away. Room lights were turned out, and the sample was lit obliquely, visually

enhancing the slight variations in surface height that were associated with the cracks. This could be done on the natural base of a sample, or on surfaces exposed through dissecting techniques. To open up a sample, and allow the study of the 3D pattern, a 20 V DC motor, attached to a thick, serrated metal disk ($\sim$3 cm diameter) sufficed. A starch plug was wrapped in tin foil for protection, and placed on a jack. The saw was held at a fixed height, and the jack raised so the starch met it. By pushing the starch against the blade, up to 2 mm of starch surface could be atomized on every pass. This allows a thorough investigation of large cross-sections of a sample at regular depths, but has significant drawbacks. It is labor intensive, messy (the dust produced requires a dust mask to deal with, and easily spreads across the whole lab if care is not taken to contain, and clean it), and very destructive to the sample. Small, submillimeter, columns cannot handle the strain of the saw, and break unevenly, while large columns can often shatter. Some care must be taken when analyzing these results.

Finally, x-ray tomography was used to get high-resolution volume filling images of starch samples. The Mouse Imaging Centre, associated with the Toronto Sick Kids Hospital, provided access to a micro-computed tomography (Micro-CT) machine (Enhanced Vision Systems, rotating-specimen system). The resulting images had voxel resolution of 36 μm^3, and allowed a detailed study of the initial coarsening and ordering of the starch colonnades. MicroView, 3D image viewing software, was used to extract cross-sections, and movies, of the primary data. Simple investigation of the data sets within the MicroView environment was also useful in developing my understanding of the 3D nature of this pattern.

Digitized images were converted to tiff format, and analyzed using Scion Image. An attempt to write Matlab code which would identify and trace over the crack network in an image was not successful. Thus, the crack network of each image were traced over by hand, in order to be analyzed. Once this was done, Scion Image was used to measure the cross-sectional areas, side lengths, joining angles, the number of neighbors, of columns.

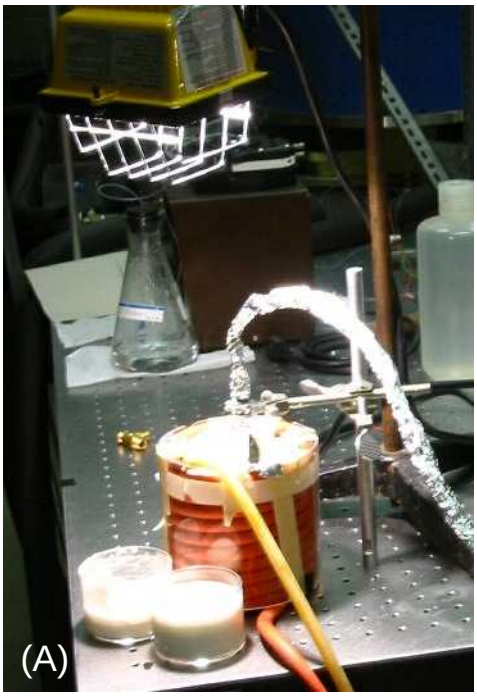

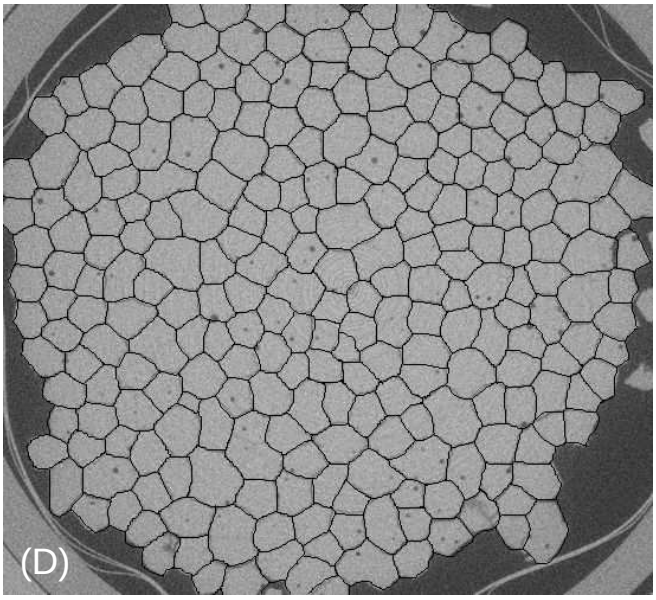

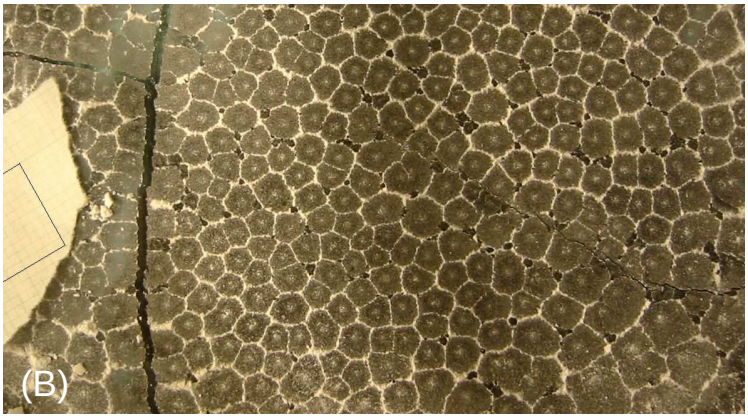

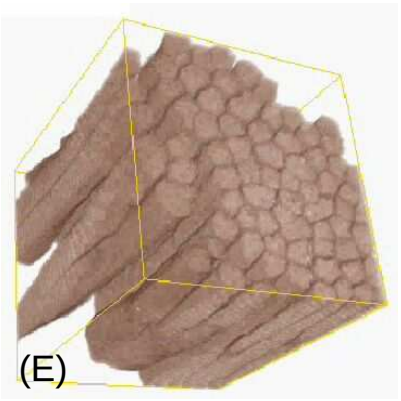

Fig. 2.1. Techniques used in data acquisition and analysis. (A) Drying setup. (B) Starch counterpart left on glass dish. (C) Cross section of partially dissected starch sample. (D) Cross section of tomograph data, with hand drawn column overlay. (E) Volume filling tomograph image.

2.2 The drying process

As the starch dries, it is split into independent plates by first generation cracks, fractures that penetrate the entire depth of the starch, as shown in fig. 2.2. The average size of these plates is depth dependant, with deeper samples often only having a single first generation crack, nearly bisecting the sample. These cracks join each other, and the beaker walls, at right angles. Frequently, they circle the beaker, running parallel to, and near to, the beaker walls.

A crack front then initiates at the surface, and penetrates into the starch over several days. These cracks form a disordered network near the surface, but mature into quasi-hexagonal columns within a few centimeters, as shown in fig. 2.2.

This front is the common surface described by the fracture tips at a particular instant, and resembles a concave bowl (it is slightly deeper at the center than near the edges of the beaker). This shape was seen by breaking open a partially dried sample, as well as by noticing that the centermost area of the counterpart appears on the base of the glass, before the area near the edges. Starch removed from just below the crack front has a remaining hydration level of 27%.

Several attempts were made to track the fracture front as it penetrated the sample, and to measure what is going on inside the starch as it dries.

2.2.1 Thermal measurements

A thermal probe was built using precision thermistors (Fenwal Electronics 120-104KAJ-Q01). The thermistors are cylindrical, approximately 1 cm in length, and 0.1 cm in diameter. 5 were arranged in a spiral around a central glass rod, at approximately 3 mm intervals, as shown in fig. 2.3. A sixth was sealed in a small metal cylinder, and acted as a measure of the ambient temperature. The six thermistors were connected to a Kiethly multimeter. A program written by Wayne Tokaruk [43] was modified to periodically sample the six channels at 60 s intervals, and outputs the resistances to a file.

The array was calibrated by immersing the probe in a beaker of ice water, along with a stir bar and alcohol-based calibration thermometer. The water was heated slowly by a hot plate, while the temperature of the thermometer and thermistors was

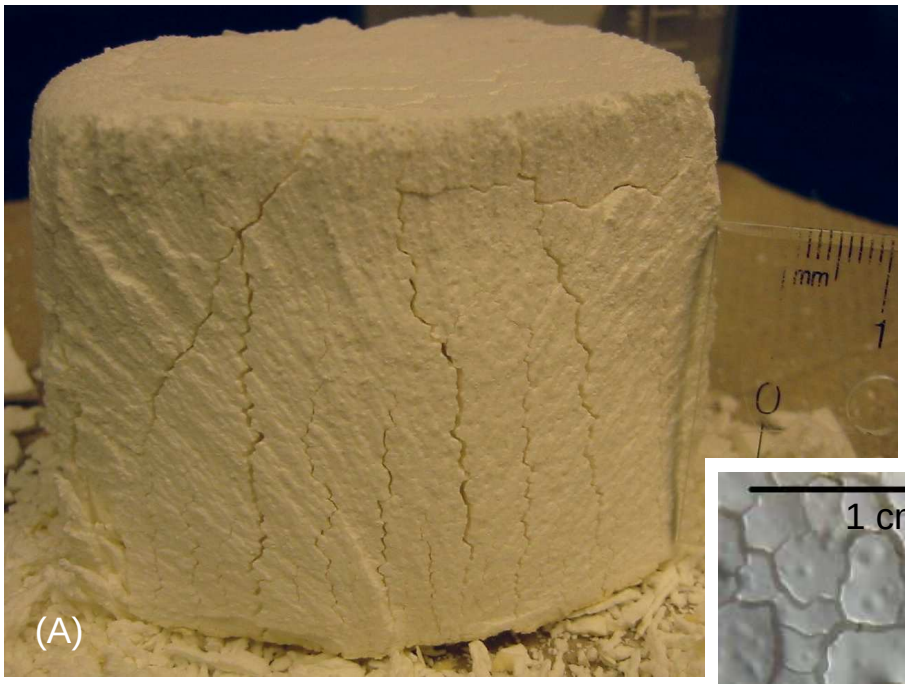

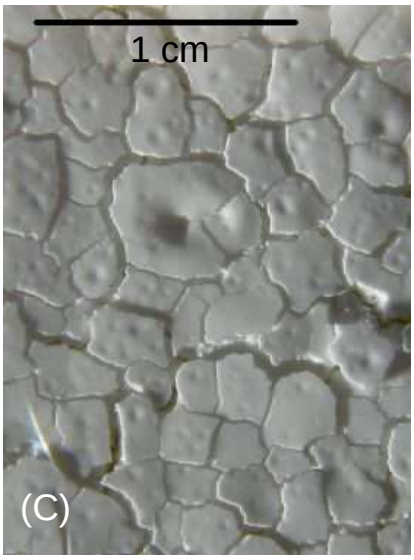

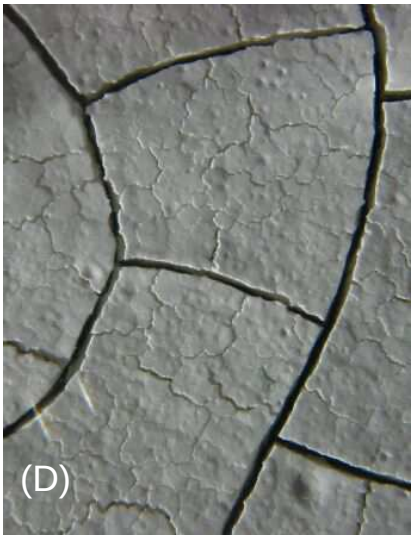

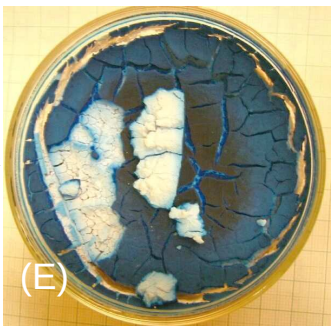

Fig. 2.2. Examples of fracture types in corn starch. (A) Plumose structure and sequential fracture on the side of a 1st generation crack. (B) Inside of a starch sample showing a well formed colonnade (drying surface is at the bottom of the picture). (C) Surface flakes form on top of the starch as it dries. They are detatched from the surface, and cover a finer, disordered, superficial crack network. (D) 1st generation cracks in corn starch break a sample into independent volumes. (E) Initially homogenous aqueous salts are deposited at the surface.

recorded from 0°C to 50°C. The data was fit to the Steinhart-Hart function

$$R = \frac{1}{A_1 + A_2 \ln(T) + A_3(\ln(T))^3} \tag{2.1}$$

for temperature T (in Kelvin), resistance R, and fitted constants A_1, A_2 and A_3. The accuracy of this fit, as shown by the accompanying residuals, is shown in fig. 2.3(C).

The array was connected to the multimeter using twisted pair wire. This posed a serious problem, as electromagnetic noise in the background made precision measurements difficult. Noise was reduced by wrapping the wires with tin foil to provide some shielding, and by subtracting out the variations picked up by the ambient temperature probe.

Several corn starch samples were dried while the temperature profiles were measured near the center of the sample. Fig. 2.3(B) shows a sample 4 cm deep, with the probe set just below the surface. To protect against fluctuations in the drying environment, the sample was dried in a tin foil container surrounded by a coiled rubber hose circulating water at a constant 25°C. A lamp was set up 40 cm above the sample, and a plexiglass draft shield was set up around the tubing.

The temperature curves, shown in fig. 2.3(A), are still noisy, but show several distinct features. For the initial 40 hours, not much happens. Surprisingly, during this time, the surface cm is almost a degree cooler than the internal starch. This can be ascribed to evaporative heat loss at the surface. The corn starch solution is somewhat translucent, and radiative heat should be able to penetrate through the cooling surface, to maintain a higher temperature in the interior of the sample. I believe that, during this period, the water in the suspension is mobile enough to move freely through the sample, within the time scale of the evaporation. Water is evaporating from the surface, but a homogeneous water concentration is able to be maintained through the entire depth of the sample.

Near 40 h into the drying process, the temperature suddenly rises in all five probes. I had hoped to be able to analyze these curves to show a phase delay in the curves, and to track a transition in temperature associated with a moving evaporation front. However, the data is not clean enough to be able to check this. It does seem, however, that no sharp temperature front will exist. By the end of the drying run, all the

probes are stabilizing into what one would expect of a thermal mass held at two fixed temperatures on opposite sides: a linear change in temperature as a function of depth.

2.2.2 Mass measurements

Müller [28] describes his measurements of a desiccating corn starch sample, weighed 25 times during a 120 h drying run. His results suggest that the drying is describable as a single phenomena, as the weight decreases smoothly.

This, however, is not the case. Using a Ohaus Scout II analytical balance interfaced with a computer, the mass of a drying starch sample can be measured as often as desired. The output of a simple program I wrote, weigh.vi (included in Appendix A), was easily adapted to measure the mass of a drying sample every minute.

In a drying run (with conditions similar to the temperature data outlined above), the mass-time curve showed two distinct drying regimes (see fig. 2.4(A)). The first is a nearly linear decrease in mass, representing the period when water can freely evaporate. This is followed by a sharp kink, as evaporation becomes dominated by diffusion or wicking. After this point, the evaporation rate slows down considerably. These evaporations can be fit to the function

$$m = A_1 + A_2 \cdot (t + A_3)^{A_4}, \tag{2.2}$$

with mass m, time t, and constants A_1 through A_4. Purely diffusive desiccation would predict this formula with an exponent of 0.5, while homogeneous desiccation would predict the same formula, with an exponent of 1. For the initial evaporation, the best fit exponent A_4 is 0.86, indicating that the evaporation rate is, indeed, nearly constant. The sharp edge in the residuals from this fit show that there is a sudden change in dominant drying mechanism. In fig. 2.4(B) a lighter sample was more quickly dried, over 200 hours. In this run, the intermediate data (25-150 h) were fit to an exponent of 0.21. This is a smaller exponent than the 0.5 that would be expected of a diffusive system, but still indicates that evaporation slows down due to the diffusive/wicking nature of the water extraction. The fit breaks down after 150 hours, as the sample fully dries out.

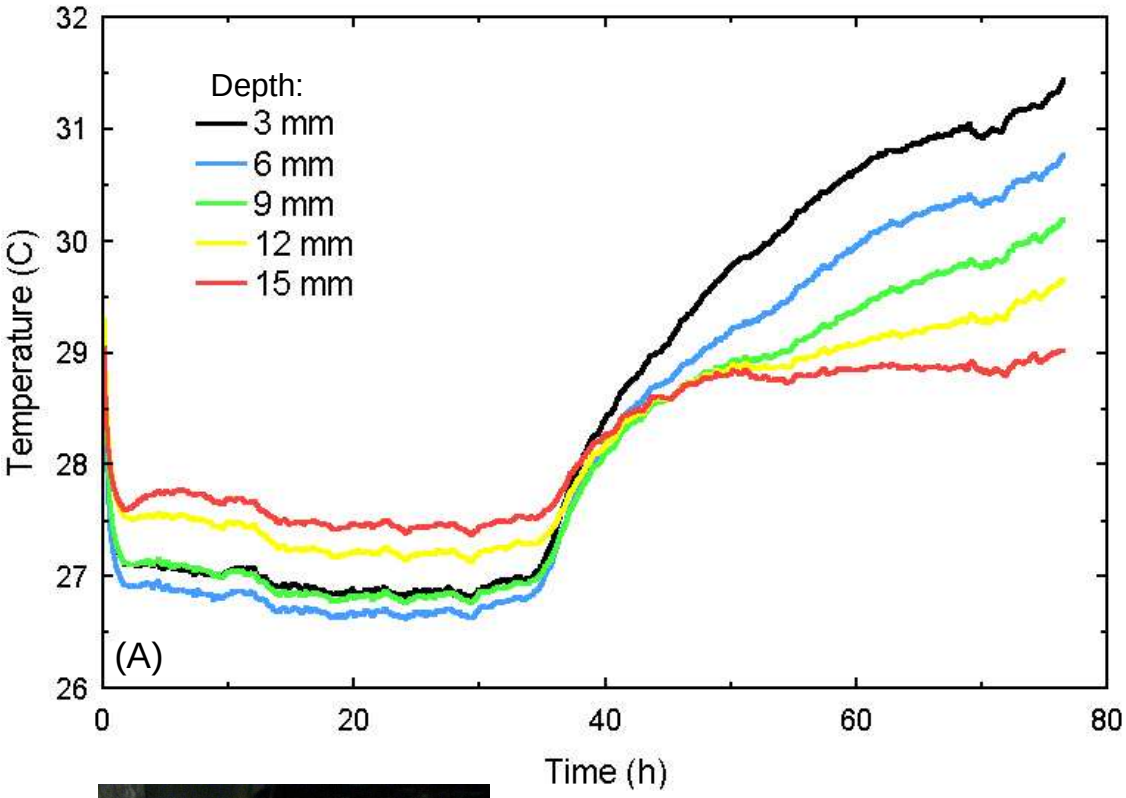

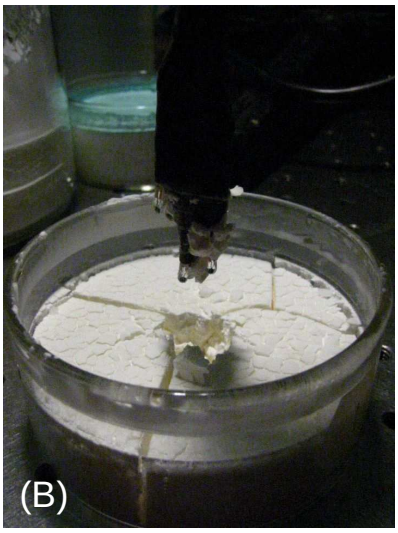

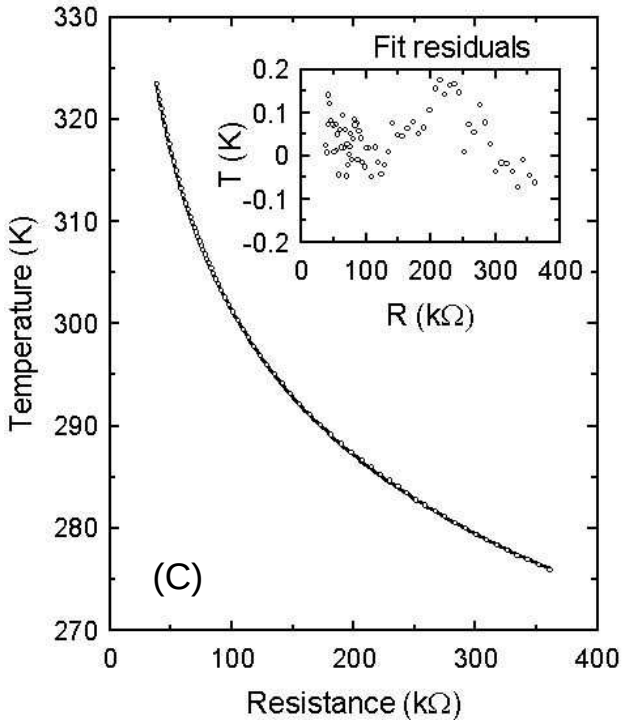

Fig. 2.3 Temperature investigations. (A) Temperature within a starch plug is seen to be dependant on time and depth. (B) Thermal probe, as just removed from a dried sample. (C) Calibration fit of a thermistor.

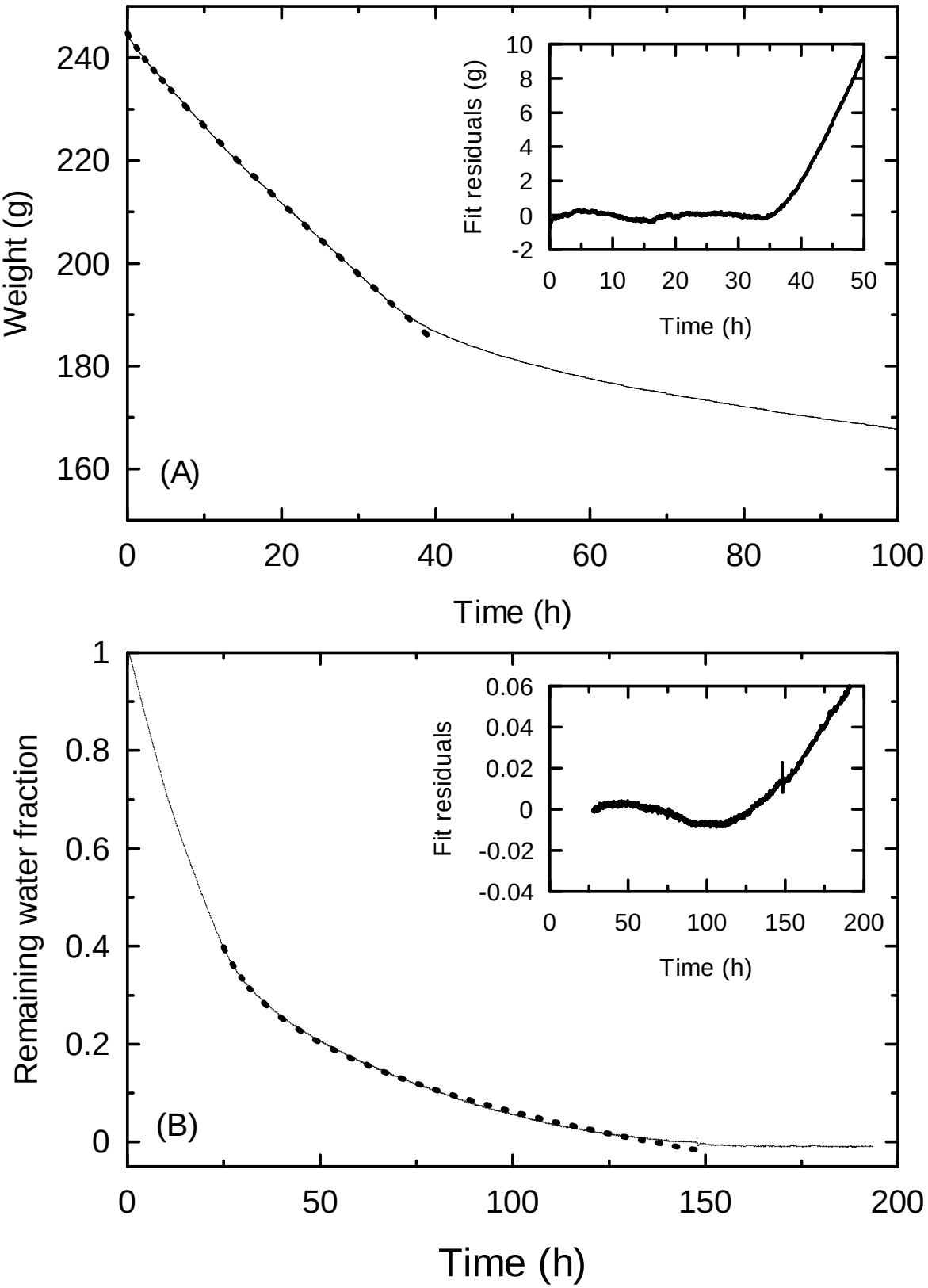

Fig. 2.4. Sample drying curves for corn starch. (A) clearly shows a change in drying character at approximately 40 h. (B) a 140 g sample dried somewhat slower, shows the long term limits of drying, and how all the water is removed during the drying.

2.2.3 Salt indicators

Two samples were grown to which $CoCl_2$ and $CuSO_4$ salts had been added. These had been originally selected to be hydration indicators, as both change color depending on the water content of their environment. $CoCl_2$ is a cobalt blue in warm or water poor circumstances, and red in cool, wet conditions. $CuSO_4$ is white when dry, and baby blue when wet. The dried $CoCl_2$ sample, with some of the surface flakes removed, is shown in fig. 2.2(E). The surface 2 mm of the sample is very heavily dyed, as most of the salt has been deposited at the drying surface. There is a slight red tinge to the remaining starch, perhaps from $CoCl_2$ that has bound to the starch, or perhaps which is incorporated into any remaining water left in the sample. No salt was left on the walls of the cracks, indicating that evaporation did not occur through the cracks. This contrasts with basalt, where water may enter cracks and boil at depth [11, 3] and suggests that particulars of the isotherms in basalt are not important to the crack pattern.

2.2.4 Discussion on the drying process

Through these experiments, I attempted to study the drying process, and the drying front. The active cracking region of a growing colonnade is confined to a thin region around this front, and the front's penetration rate and width (from the top to the bottom of the crack front) are important variables which likely help determine the scale of the crack pattern. These experiments do not shed quantitative light on the nature of this front, but some understanding can be gained by combining the qualitative results.

First, it is obvious that there are two distinct drying periods, each producing a distinct crack pattern. By looking at partially dried starch throughout the temperature and mass experiments, it seems that the initiation of the quasihexagonal crack front is coincident with the jump in temperature within the starch, and with the kink in the mass-time relationship. This means that, initially, the starch almost certainly dries homogeneously. Cracks forming during this period are large, and break the sample from the drying surface to the base. Müller has observed these first generation cracks, and claims that they form quickly, with crack tip velocities ranging from mm/min.

to cm/s [28]. Plumose structure, visible as the feathery pattern in fig. 2.2(A), show that these fractures start at an epicenter (usually at the drying surface), and radiate throughout the sample. Columnar jointing is confined to the second phase of drying, when a clearly established crack front exists, and when the mobility of water in the starch is much reduced.

Next, these experiments do shed interesting light on the drying mechanism during columnar jointing. It is likely that capillary action, the wicking of water within the starch slurry, is the dominant drying mechanism, rather than the diffusion supposed by Müller [28]. The exponent in the decrease of the drying rate is not that expected of diffusion, but much lower. Further, it is not obvious that water, escaping starch by diffusion, would leave salt solely at the surface. However, capillary action's well known ability to transport solutes forms the basis of chromatography, an analysis technique that separates solutes based on their mobility. With water evaporating at the surface, there would be a pressure gradient established which could drive such capillary motion.

Finally, comparing these results to what is known of columnar jointing in other media, it seems that the specifics of the driving force behind the shrinkage cracks does not greatly affect this pattern. Known examples exist where shrinkage is caused by diffusion through the bulk medium (ice [25], and possibly certain basalts), convection through the cracks (basalt cooled by water seepage [11]) and through capillary action. Any of these shrinkage mechanisms could produce sequential cracking, and a finite-width fracture front. Within certain unknown limits, this may be all that is required for columns to spontaneously form.

I am continuing the work of investigating the drying characteristics in starch, and some promising experiments are described in chapter 3.

2.3 Crack Patterns

The main thrust of this research is the description of quasihexagonal crack patterns in a quantitative manner. Despite the long history of scholarship regarding basalt, hard data concerning this pattern are rare. The data presented in this section agree with statistics gathered on this pattern in basalt, when available, and extend upon

them in several ways. Most importantly, these represent the first description of the evolution of this pattern in all of its three dimensions. These observables can, in future work, be used to discriminate between competing theoretical treatments of columnar jointing.

The ordering and coarsening of columnar joints in corn starch were studied in detail in 20 samples. The first, a 2.5 cm deep sample, was analyzed by Micro-CT techniques. The next two samples (6 and 10 cm deep) were sawn open at 2 mm intervals throughout their depth, with data captured using digital photography. These first three samples were dried with the heat lamp between 10 and 20 cm of the starch's drying surface, with initial drying rates of approximately 30 mg cm^{-2} h^{-1}. The remaining data set was gathered by imaging the counterparts left on the bottom of the glass dishes after the dried starch plugs were removed. 17 samples of different depths were dried in this experiment, with the drying conditions at an initial 10 mg cm^{-2} h^{-1}.

2.3.1 Edge effects: Container walls and first generation cracks

The crack front in a beaker of starch is not a horizontal plane, propagating through the starch – it curves up near the edges of the container, since the removal of water vapor is inhibited near these walls. There may also be some effects arising from the way the starch sticks to the glass walls, as well as in the way that cracks interact with this boundary. In any event, the patterning of the starch cracks near the glass walls of the containing vessel are different from the cracks within the interior of the sample. The polygons are larger, and the pattern is less well formed. The cracks meet the walls at right angles, as they must when they join a free surface. Therefore, during data analysis, I have usually neglected results near the edges of the sample. In situations where a sample, in cross section, only contains a few large polygons (all of which need to be counted to reduce statistical error), all polygons in contact with the boundary, as well as their neighbors have been neglected. In other samples, when there are enough polygons to make the collection of large data sets easy (and this is most often the case), I have preferentially analyzed the crack patterns near the center of any sample.

The columns bounding first generation cracks are distinct in that, on average, they

form pentagons, rather than hexagons. Since the surface of the first generation crack is a free surface, the nearby starch can contract in the direction normal to it. The stress field near such a surface implies that new cracks join to it at right angles. The remaining vertices, away from this joint, form the 120° angles expected in columnar jointing. Some such joints can be seen in fig. 2.1(B) near the left hand side of the image. For these reasons, when analyzing data, columns bounding first generation cracks have also been neglected.

2.3.2 Ordering of the crack pattern

One question regarding columnar jointing is how a disordered network of surface cracks orders itself. Surface cracks in lava predominantly join at 90° angles [32]. In this they are similar to shrinkage fracture patterns in thin layers, where local stress fields dictate that cracks should intersect at 90° [41]. Joint angles studied at the Boiling Pots basalt in Hawaii show that, within a meter of the base of a flow, the majority of 90° junctions have smoothed out to angles between 100° and 140° [1]. This is a remarkably quick evolution, as the mature colonnade has an average edge length of 30 cm, and explains why the ordering is so easily overlooked in a field study. Other studies have noted a narrowing of columns within 2 m of the surface of certain lava flows [32, 10].

The surface of a dried corn starch sample is covered with thin superficial flakes, which are unattached to the bulk of the sample. Based on the experiments with salt indicators, it is likely that these flakes are the result of impurities in the stock corn starch, and would be difficult to eliminate. However, these flakes make it difficult to visually inspect the surface cracks of the bulk sample. Even after peeling the plates away, the surface crack network is far too fine to resolve by eye, and too rough to produce meaningful imagery.

This is the situation where high resolution tomography has been especially useful. A sample roughly 2 cm in diameter, and 2.5 cm deep was analyzed, which was large enough to produce meaningful statistics for the small near-surface columns. The cross-sectional area, number of neighbors, and distribution of joint angles were measured in cross-sections taken through the volume, at 1.78 mm intervals. The most informative results are summarized in fig. 2.5. Here, fig. 2.5(A) shows how the average cross-

sectional area increases smoothly in the entire sample. An exponential power law, to be discussed later, has been fit to the data. Note how there is a finite, yet very small, scale that is natural to the pattern as the depth approaches 0. Fig. 2.5(B) shows how the relative variation (the standard deviation divided by the mean) in the average area decreases as the pattern matures. Fig. 2.5(C) shows how the the abundance of Y-joints, which I have somewhat arbitrarily defined to be those closer to a 120° joint than a 90° joint, stabilizes with depth. Fig. 2.5(D) shows the variation in the number of neighbors as a function of depth. Figs. 2.5(E) and (F) reinterpret the measurements of angles, and show histograms of the distributions at 1.4 mm and 18.2 mm depth, respectively. These histograms are very similar, and peaked around 120°, prompting a measurement of the variance of their distribution, included as fig. 2.5(G).

The network is surprisingly ordered even at the very surface of the sample. Within 1.5 mm of the surface, a depth comparable to the scale of the initial crack network, a number of features familiar to hexagonal jointing are visible. The network already has a great number of Y-joints, and the distribution of angles clearly peaks at 120°. The average number of neighbors for any column is precisely 6, within statistical error, throughout the entire sample. This is necessary for any crack network lacking X-joints, the vertices of 4 distinct cracks [9].

All the statistical measurements meant to characterize the disorder in this pattern stabilize within the first cm of the sample. The relative variation in the cross-sectional area declined from 0.5 to 0.3. This suggests that there is some process acting to equalize the areas of adjacent columns. The distribution of joint angles also smooths out, as the majority quickly become well formed Y-joints. Further, variation in the number of neighbors, initially peaking at around 1.1, settles to a stable value of 0.8. All this implies a strong tendency towards uniformity in every measured aspect of this crack pattern.

It has been customary to report distributions in the numbers of sides of individual columns. The variance in these distributions usually range from 0.8 to 1.3 [3], with the well formed columns of the Giant's Causeway setting the lower bound of 0.8. However, the edges of starch columns, especially near the surface, or when columns merge with each other, are not necessarily straight, and thus the number of neighbors

is a more well defined variable.

All of this ordering occurs while the pattern is still changing it's scale. This implies that a crack network may mature into what can be described as a quasihexagonal fracture pattern before it reaches a stable column scale.

2.3.3 The pattern scale

The single most interesting question to be asked about this pattern is, what sets the scale? Why can basaltic columns be meters wide, starch columns millimeters wide, and ice columns microns wide? Even these figures may be misleading, as basaltic columns have been reported as small as 1 cm in diameter [31], and upwards of 2 m [10]. What provokes such variability? It is thought that, in basalt, the cooling rate determines column size [10, 23]. In starch, analogously, the evaporation rate determines the pattern scale, as has been shown qualitatively by Müller [28].

There are good reasons for this. There are only 2 length scales natural to columnar jointing. These scales are associated with the column area (or alternatively the perimeter length, average side length, column diameter, or any such equivalent measurement which has been made), and the striae width. The striae size preserves the width of the fracture front, and is usually between 5% and 20% of the side length in basalt [10, 37]. These two length scales may be inherently linked. The width of the crack front should be determined solely by the rate of evaporation (or cooling rate), the front's penetration speed, and material properties. These properties should be the thermal diffusivity and specific heat of basalt, and the analogue properties of starch.

In starch, as we have already noted, the evaporation rate decreases dramatically throughout the experiment, albeit in a smooth manner. Simple early experiments varying lamp height confirmed that slower drying rates lead to larger columns. A set of more precise experiments comparing the incident power shining on the starch to the column area at a constant depth have been carried out by Lin Zhenquan, in collaboration with this work [48]. These experiments showed that area is related to drying power by a inverse power law with an exponent of 2.2 [48].

Other experiments were done by adding gelatine to the starch slurry, and letting it set before drying. Less than 0.5% gelatine by mass could significantly change the

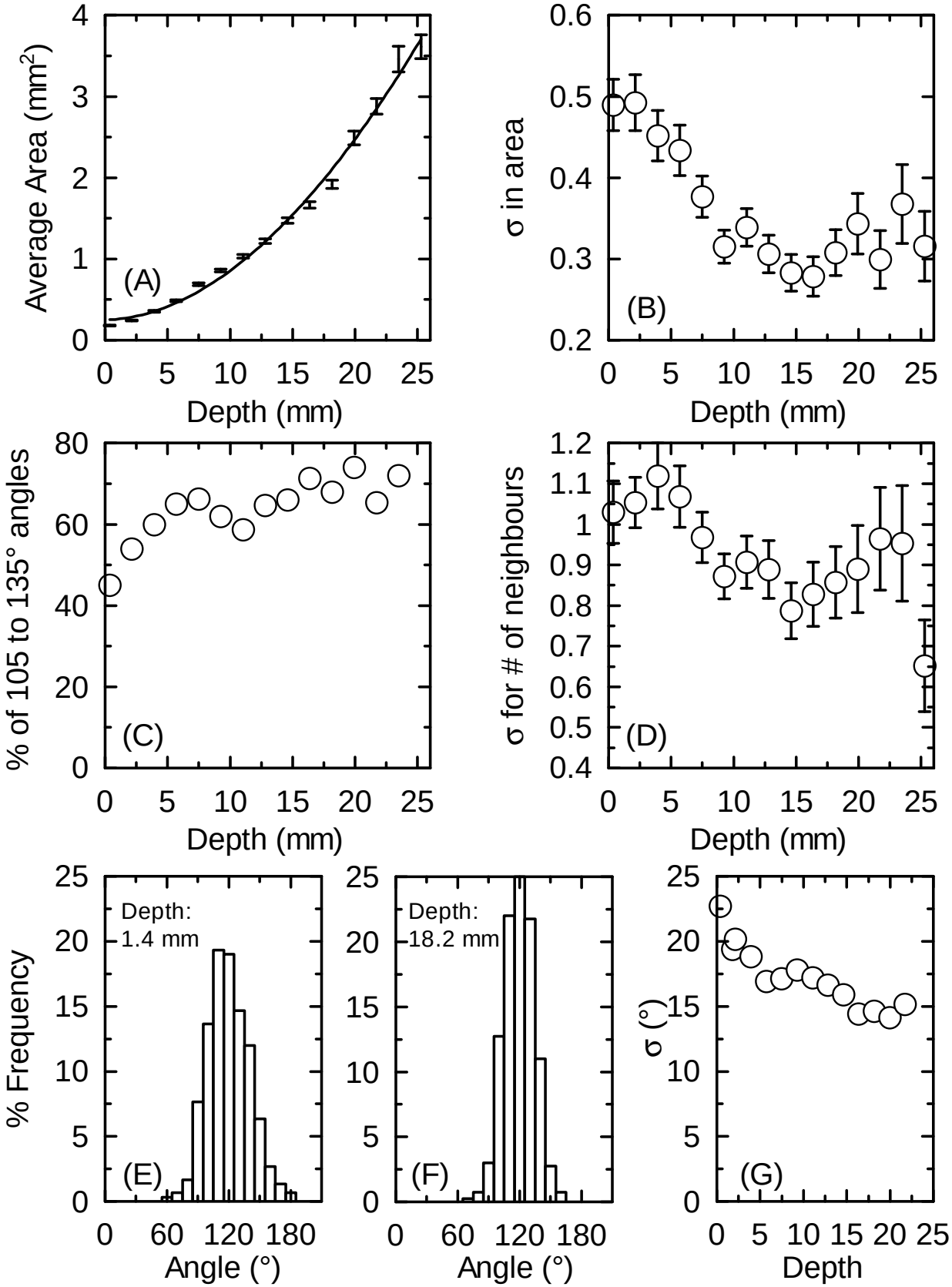

Fig. 2.5. Statistics showing the ordering of a starch colonnade near the drying surface. (A) shows the smooth increase in cross-sectional area of the tomograph data, while (B-G) show how the pattern becomes ordered within the first cm.

material characteristics of the mixture, making it much stiffer. An early observation that the pattern scale increases with gelatine concentration has been confirmed by Lin Zhenquan [48] whose experiments have since quantitatively probed this relationship.

I have performed a detailed study of the depth dependence of the cross-sectional area, which was measured in all 20 of the recorded samples. 2 very different types of coarsening which occur in these samples, as seen in fig. 2.6. The normal mode of coarsening is well described by a power law, where the exponent varies from 1.4 to 2.2. This exponent was tested in five parts of the data, as summarized in fig. 2.6. Although the error bars of the fits do not overlap, there is no clear trend to the distribution of exponents. It is conceivable that there is a single general power law governing the coarsening of this pattern, but with such a range of exponents, running over only 1 1/2 decades of data, this is not obvious.

However, in two data sets, sharp increases in scale occur between regions of the normal, more leisurely coarsening. This transition region is only 0.5 to 1 cm deep, and shows an increase in some parameters used to characterize the disorder in this pattern: the variance in the number of neighbors, and in the cross-sectional area, as shown in fig. 2.7. In the 6 cm deep sample, the variance in the number of neighbors reaches 1.2, while a value of 1.0 is observed throughout the transition in the 10 cm sample. In fig. 2.7(B), it is shown how the variance in the cross-sectional area of these columns is raised in the transition region.

These jumps in column scale cannot be explained by edge effects – a response of the pattern to the bottom of the container – as changing the total depth of the starch sample did not affect the transition. Nor can they be explained by appealing to uneven drying conditions; recall the experiments with colored salts and the mass measurements. All results argue towards a smoothly decreasing drying rate, driven by simple processes.

I think that it is the geometrical nature of the pattern itself that provides a solution: the pattern partially resists anything but catastrophic changes in scale. In a mature starch colonnade, most columns' area lies within 30% of the average. A study of the tomograph volumes indicates that fracture termination is the dominant mechanism of increasing pattern scale. The termination of a joint between two hexagonal columns will create one large octagon, and leave two neighboring columns as pen-

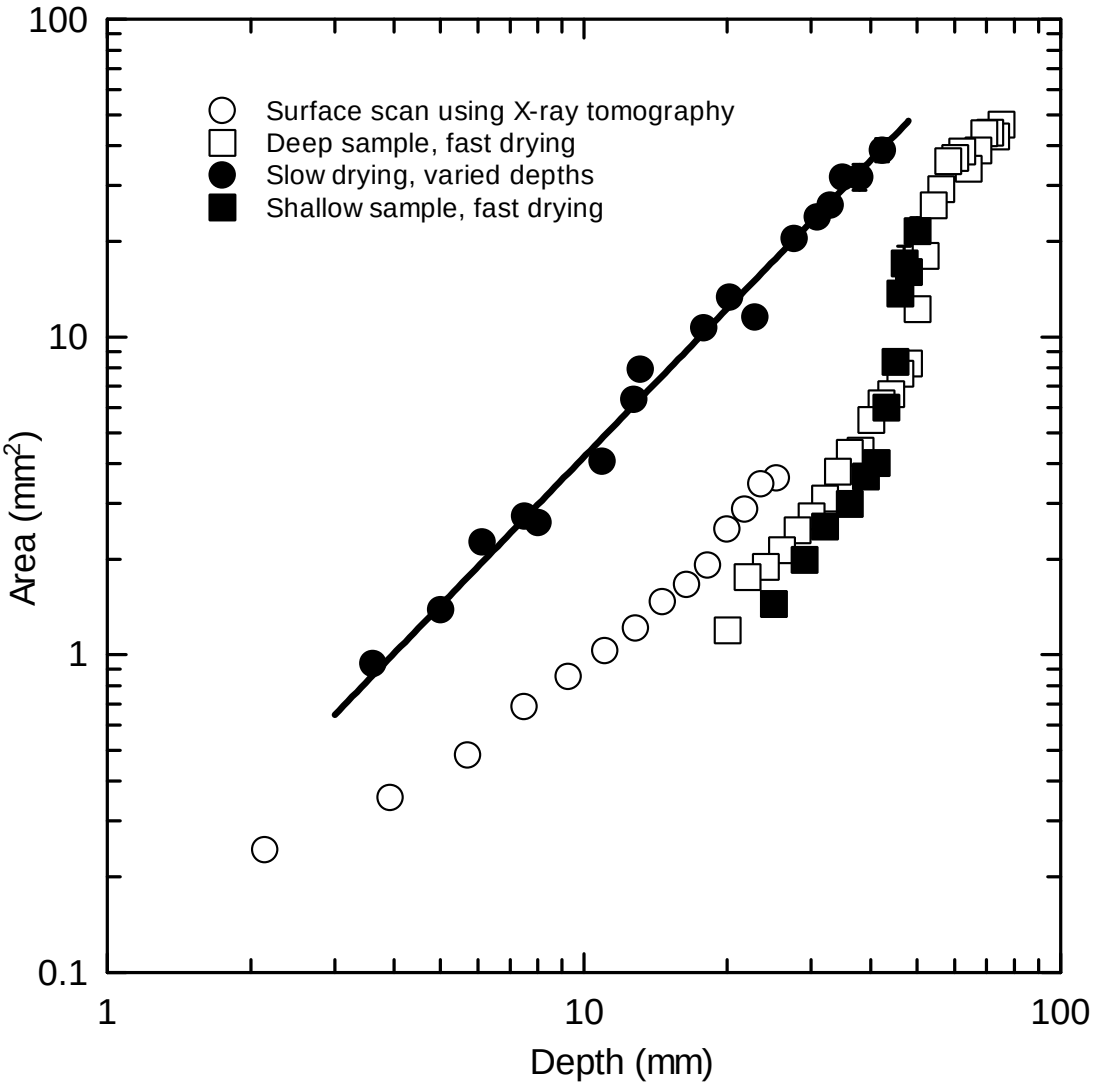

Sample description	Exponent
Surface scan using X-ray tomography	1.94 ± 0.13
Deep sample, fast drying, before jump	2.26 ± 0.07
Deep sample, fast drying, after jump	1.42 ± 0.20
Slow drying, varied depths	1.55 ± 0.07
Shallow sample, fast drying, before jump	2.01 ± 0.07

Fig. 2.6. Coarsening in corn starch falls into two regimes. The usual coarsening can be fit to a power law with exponents of 1.6-2.2. The fit shown has an expoent of 1.6. The other type of coarsening is a sudden dramatic change in column scale, as shown in the jumps in the fast dried data, near the right of the figure.

tagons, increasing the disorder in the pattern as well as increasing the scale. Whether any particular joint will terminate or advance depends on whether the current crack pattern, or one with a single column spanning the area currently occupied by two columns, is more favorable. Thus, as long as the current pattern is more favorable than one with (approximately) double the average area, it will remain stable. This implies that, for any fracture advance rate, a range of pattern scales will be stable. The particular scale observed will depend on the history of the pattern, and the crack front. Further, when the pattern becomes stressed enough such that normal columns begin to merge, the shift in scale will be dramatic. Due to the regular column size in the fracture network, one terminating joint implies an abundance of similar, unstable joints. Such a hysteretic pattern has been reported in thin film crack patterns [41].

If this is true, it still requires some explanation of why the colonnade can coarsen by the slower, more common mode. There is a residual disorder in this pattern after columns have formed. All the gathered statistics describing disorder are constant through the sample, apart from the initial ordering region, and from these sudden scale changes. Moreover, the constant 0.8 in the variance of the sides/neighbours agrees with the most ordered basalt formations [3]. Neither basalt, nor starch, seem to become more ordered as the columns form. This residual disorder implies that, as long as the pattern is not in its ideal scale, there will likely be a few scattered columns capable of merging, in order to adapt the pattern to a more appropriate scale.

2.3.4 Correlation between angles and sides

By reanalyzing O'Reilly's survey of the Giant's Causeway [30], Weaire and O'Carroll found a linear correlation between the length of joints, and their terminating angles [46]. Based on their data, and on the observation that as X-joint, with four edges joining at 90°, is effectively an edge of length 0, they suggested the empirical relationship

$$\theta = 90^\circ + 30^\circ \cdot L/L_{mean} \tag{2.3}$$

with L and θ as in fig. 2.8(B). This was in 1983, and they used the result to argue that such a strong correlation was unlikely to arise in the then popular description of the Causeway's formation. The same structure has been reported in the Devil's

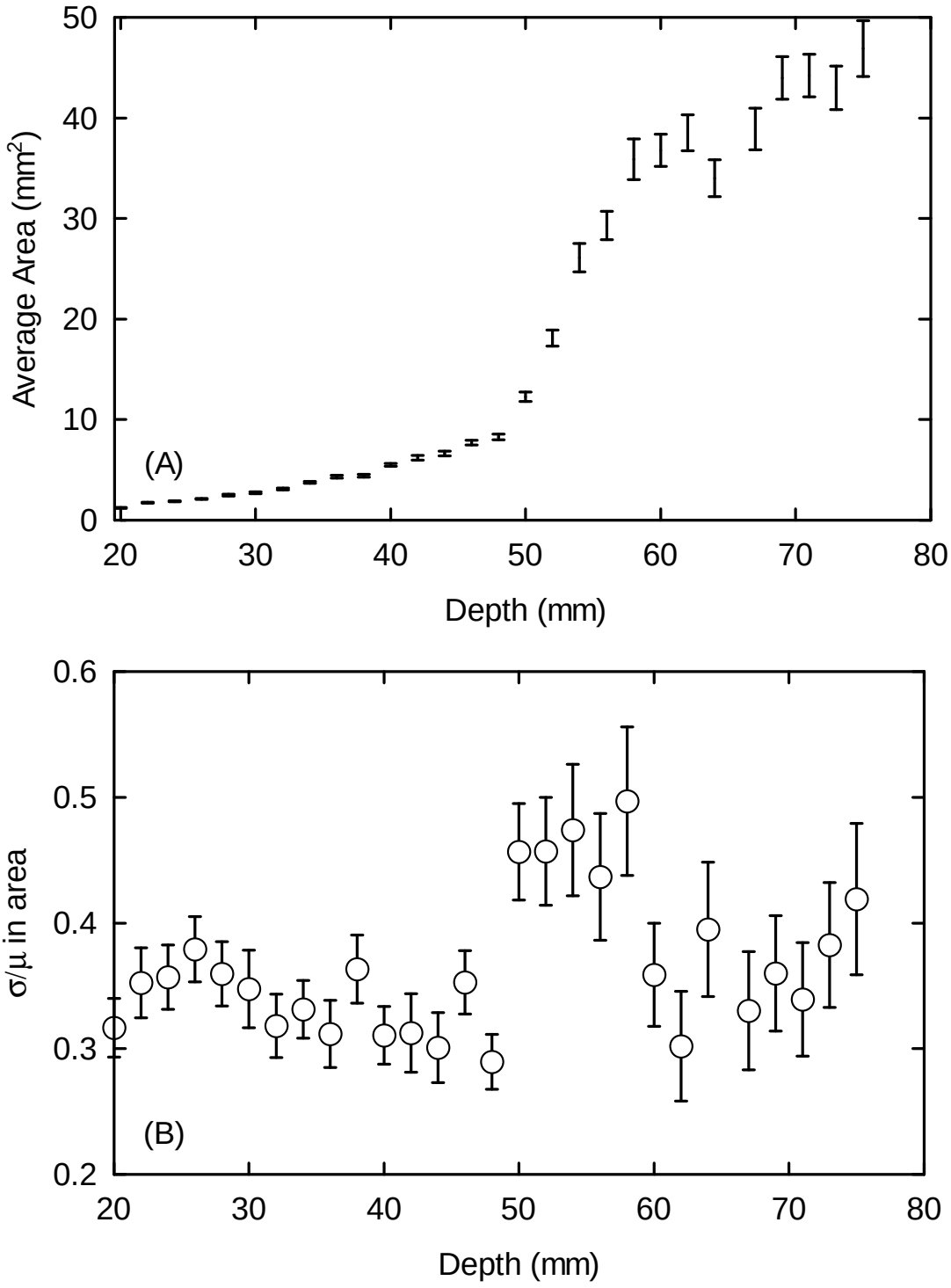

Fig. 2.7. A transition region in a deep sample. (A) The cross-sectional area of a 10 cm deep sample increases suddenly between 5 and 6 cm. (B) In this region, there is an increase in disorder, as shown by a jump in the relative variance of the cross-sectional area.

Postpile [1].

To test whether this correlation held in starch, 70 column sides were measured, along with the angles at their head and tail (L and θ as shown in fig. 2.8(B)) from each of 4 different depths: a cross-section at a depth of 41 mm in the fast dried 6 cm deep sample, and cross-sections of the tomograph at 3.9, 11.0, and 21.7 mm depth. The first represents a mature colonnade, just before a large jump in scale, while the last three represent the pattern as it becomes ordered. To simplify matters, an average of the angles opening at both ends of each edge were used. As shown in fig. 2.8(C), a correlation is seen in both mature and immature corn starch colonnades. There is no depth dependence.

Unfortunately, however, this interesting relationship cannot reasonably distinguish between competing theories. The original paper errs in claiming that is not a general feature of crack networks. Indeed, it can be derived by simply considering any crack network favoring 120° angles. Consider the edge and two vertices, as shown in fig. 2.8(B). Let the average length of an edge be L, and the edge of a particular joint be L′. We want to see how, by deforming a vertex with three 120° angles, the relationship between L′ and θ will change. The figure shown has fourfold symmetry, and is more easily manipulated in the form of fig. 2.8(D), where $\phi = \theta/2$. To form a first approximation to the relationship between L′ and θ, we can fix the endpoints of this figure (open circles), and allow the vertex (solid circle) to move horizontally in the figure, yielding

$$\tan(\phi) = \frac{\sqrt{3}}{2 - L'/L}. \tag{2.4}$$

This equation can be linearized, but the fit is then degraded, and only appropriate near L = L′. Both the tangent fit, and that suggested by Weaire and O'Carroll are shown overlaid on the starch and Causeway data. As can be seen, this relationship, derived purely from the geometric principles, matches these data superbly, and explains the origin of the observed correlation.

2.3.5 Pattern evolution

One of the benefits of high resolution tomography is that, by panning through the data, you can get an immediate visual understanding of how columnar joints evolve,

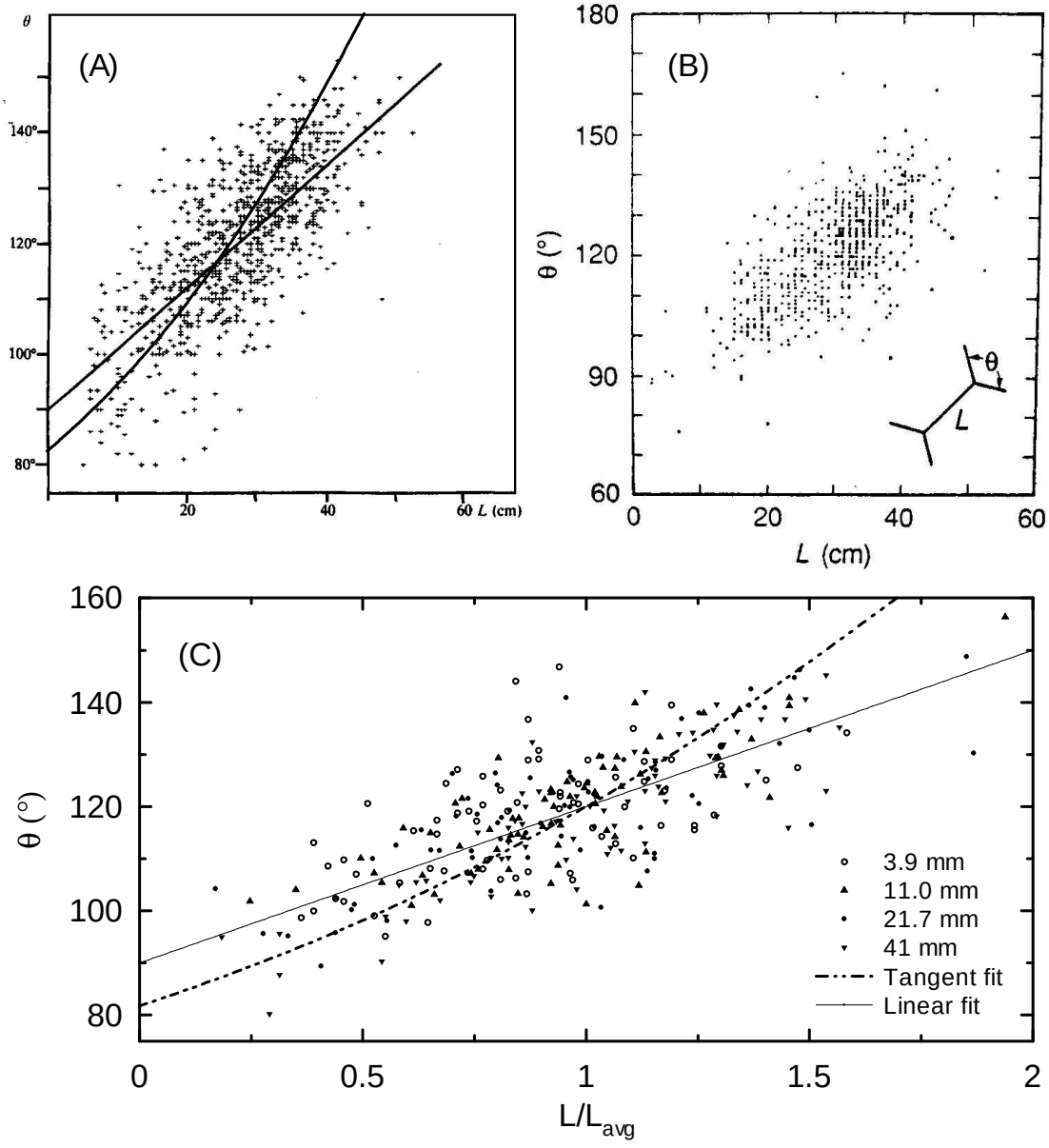

Fig. 2.8. Correlations between sides and angles. (A) Correlation in the Giant's Causeway (modified from ref. [46], fig 2). (B) Correlation in Devil's Postpile (ref. [1], fig 9).(C) Correlation in a mature starch colonnade. (D) Definitions of L, L', and ϕ. The figure represents half of a symmetrical vertex, where the white points are fixed, and the black point can move horizontally.

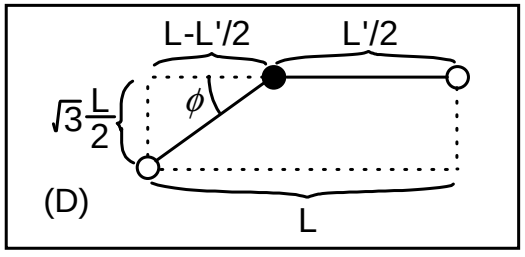

how the cracks wiggle and move, how the vertices jostle, and how neighboring columns interact. This experience is best transmitted through a movie (and one is available for download at www.physics.utoronto.ca/∼goehring/starch2.avi), but I have tried to show the essential details of this pattern's evolution in a series of slides, taken from the tomograph data, each 0.356 mm apart (corresponding to 10 voxels). Two such series are shown in fig. 2.9. Note how much the position of a vertex, or the length of a side can change in this scant space. Yet when columns are removed and looked at individually, this mobility is less apparent.

If topological changes from a perfect hexagonal lattice are called defects, then at least three kinds of defects can be identified, each giving a certain character to this pattern. The first, a pentahepta defect, has been well known in basalt [17, 3]. This defect is caused by the merging of two vertices, and the extinction of an edge, followed by their departure in a different direction (and the creation of a different edge). In a perfect hexagonal lattice this changes four hexagons into two pentagons and two heptagons. The second type of defect, already mentioned, is caused when a crack disappears, leaving a large octagon and two pentagons. As shown in 2.9 this leaves uneven edges, which are eventually smoothed out. The third type of defect is when a new column is created at a vertex. In my experience, this is most common around pairs of nearly touching vertices, and so the nascent column begins as a quadrangle, rather than a triangle. In cases where a crack front speeds up, this could be the main mechanism for decreasing the pattern scale.

2.3.6 Discussion on crack patterns

There are no such thing as X-joints. Recognition of this fact in columnar crack patterning is crucial. In thin films, an X-joint would require two cracks to connect to an existing crack at exactly the same point. Given that both sides of the existing crack are physically separated, there can be no communication between the sides of the crack, and an X-joint can only be the result of coincidence (literally). Even in 3D crack patterns, an X-joint would either require perfect coincidence, or a novel description of crack formation. While this in itself is not a proof, the observed mobility of vertices in the tomograph data argues that, at best, X-joints are instantaneous. It is necessary to form a X-joint as an intermediate step towards the creation/destruction

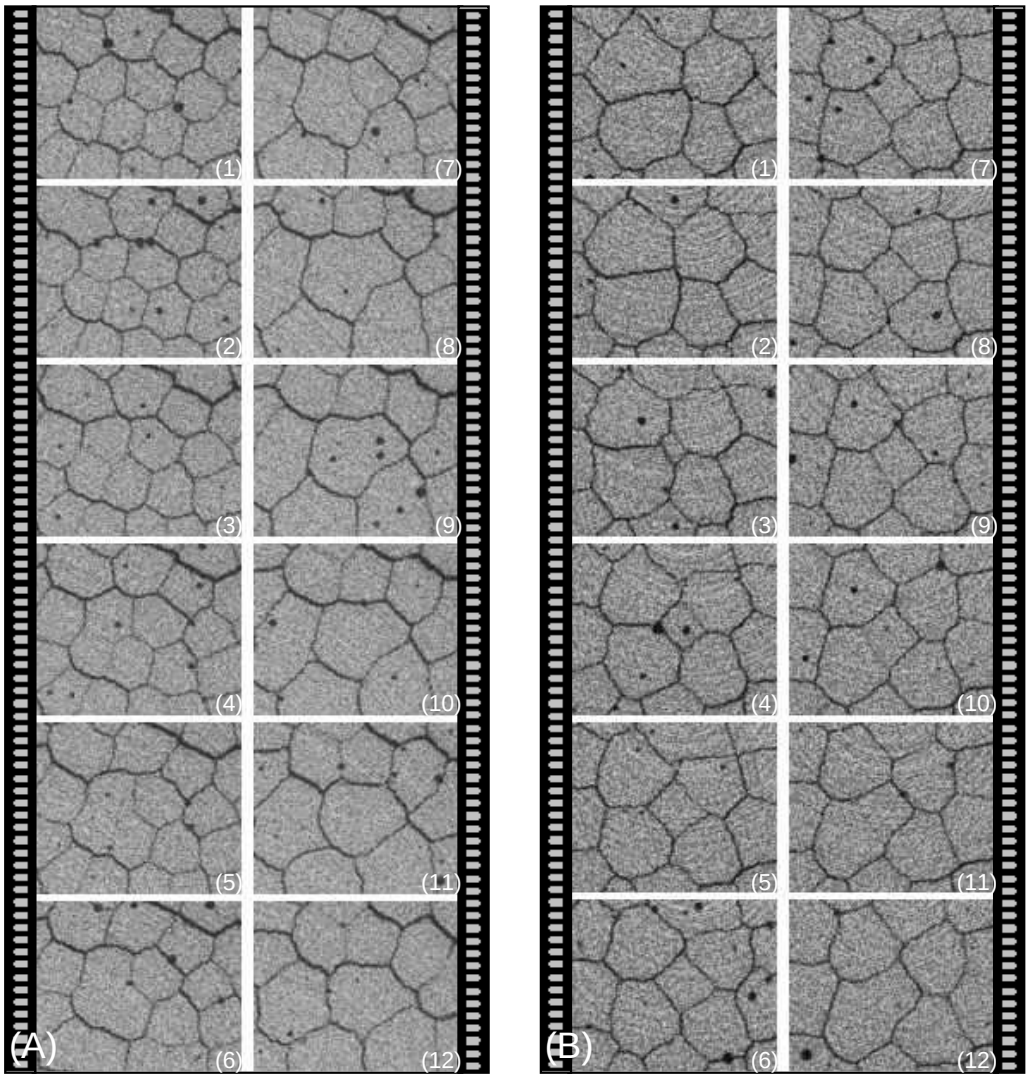

Fig 2.9. Examples of evolution of the crack pattern taken from tomograph data. Images are 0.356 mm apart, wrapping from the bottom left to top right. As the columns grow into the starch, the evaporation rate decreases. Columns size depends on evaporation rate. To compensate, columns may merge. (A) From 11.0 mm to 15.0 mm depth, showing a good example of merging. The cracks joining the three middle-left columns fade and disappear, followed by that joining a fourth column. Note how the remaining edges even out in the last 5 slides. In slides 4 to 7 the top mid-right vertices meet and swap directions, as they do when they form a pentahepta defect. (B) From 13.2 mm to 17.1 mm, showing the birth of a new column at a vertex, followed by its merger with a neighbor. As vertices shift, they can form instantaneous X-joints, as the top right vertices do in slides 3 and 5.

of a pentahepta defect. Such defects do form, and vanish, but the intermediate step is not stable. In no case have I been able to track a mobile X-joint through successive cross-sections. Further, if X-joints were stable, they should tend toward four symmetric 90° angles (recall how my statistics have tended towards homogeneity). On the other hand, if they are pairs of distorted Y-joints, then, in the relation I derived between joint angles and side lengths, the opening angles associated with vanishingly small sides should be 82°. It is clear from 2.8(A-C) that, in the limit where the side length vanishes, the associated angles dip significantly below 90°.

It has been shown that the average number of sides in an infinite plane tiled with polygons obeys the relation

$$\bar{n} = \frac{2(2J_T + 3J_Y + 4J_X)}{J_T + J_Y + 2J_X}, \tag{2.5}$$

where J_T, J_Y and J_X are the frequencies of T-joints, Y-joints, and X-joints [9]. If we are instead interested in the topology of neighbors, this can be simplified. The starch pattern lacks X-joints. Further, crack cannot cross themselves, so any network of curved sides can be continuously deformed into a tiling of perfect polygons. Finally, when considering neighbors, a T-joint becomes the special case of a Y-joint. This reduces eq. 2.5 to the claim that any crack pattern will, inherently, have an average of 6 neighbors per column. With Y-joints, three cracks meeting at a vertex, there is an average of 120° between any two cracks. This is true even at T-joints, where two 90° angles are balanced out by one 180° angle.

We have seen how the crack pattern evolves as it penetrates the shrinking medium – angles, areas, vertices and edges are all variables, and subject to constant motion. Yet, the data show consistency: the counterparts of 17 different samples gave very little scatter around their power law trend, and the two observed jumps in scale (in samples with similar drying rates) occur at almost the same depth.

The active cracking region of a growing colonnade is confined to a thin region around the fracture front. As the initial network is thus composed of a set of planar shapes possessing six neighbors, and whose common vertices are no longer forced of occur at right angles, all that seems to be required to mature a surface patten into a hexagonal lattice are conditions favoring the straightening of edges, and the

equalization of column areas. This simple driving force evidently exists, as there is a natural tendency to homogenous conditions in every statistic I studied. The particular theoretical basis for this ordering is controversial. There is, of yet, no well tested theory governing the formation of quasihexagonal crack patterning. It can be hoped that the results of this report can help discriminate between the competing theories.

Chapter 3

Ongoing research and future directions

There are several projects which I have begun, but which have not yet produced significant results. The most important of these is a system to control the evaporation rate through a feedback loop. Recall how the parameters which should determine the crack pattern scale are the evaporation rate, front speed, and the starch's hydrodynamic properties. The material properties of starch are easily changed, but so far control of the evaporation rate has only been achieved by changing the light-starch distance. If the evaporation rate can be controlled, and the front speed measured, I may be able to start investigating the origins of the pattern scale.

To do this, I have written a set of virtual instruments using Labview. These are included in Appendix A, and allow one to communicate with an Ohous Scout II balance and a triac switch. In this setup, a beaker of starch is placed on the balance. Its weight is logged every minute using weigh.vi, via an RS-232 cable connecting the scale to the computer's serial port. The starch is dried by a pair of overhead heat lamps, and an 120 V overhead fan. These are held in place on a retort stand, about 20 cm above the starch, with the fan directly overhead, and the lamps symmetrically offset by about 10°. Two triac switches were constructed using optoisolators, and controlled through the computer's parallel port. One switch controlled the fan, the other the lamps. These switches run a computer-timed duty cycle with a 60 s period. The drying rate of a full duty cycle is almost 5 times higher than the drying rate of

the zero duty cycle.

In the experiment as currently set up, the main program (evaporation control v2.vi) attempts to fix the evaporation rate to a constant. The initial conditions are a lamp duty of 0.25, with the fan turned off. To account for the kink in the drying rate, the initial drying rate is first measured, and the time of the kink predicted. 5 h after the predicted time (to make sure the kink has definitively been passed), the evaporation rate is measured hourly. The first of these measurements sets the desired evaporation rate. The duty of the lamp is then adjusted hourly, by an amount proportional to the difference between the desired and measured evaporation rates. Once the lamp has reached a full duty cycle, the fan duty is adjusted in the same manner. Once the fan is at a full duty cycle, the experiment logs the time, and shuts down.

Currently, a stable version of the software control has been written, which is designed for easy adaptation to any desired algorithm of evaporation control. Initial testing has been successful, and the sole remaining problem is in choosing the precise setting of the feedback strength. By setting this parameter too high, the experiment becomes unstable and the evaporation rate becomes an exponentially growing oscillation about the desired rate (which, however, proves that the feedback is working). With too low a setting, the feedback is insufficient to maintain a constant evaporation rate. As a modification to the current program I am considering the addition of a dynamic control of this feedback parameter.

Once this system is working, I will be able to do a number of interesting experiments. I will be able to study the evolution of the pattern scale as a function of the evaporation rate. I will be able to see if the pattern becomes more ordered in the absence of a need to adapt scale. I can attempt to drive a sudden shift from a large scale to a smaller one by suddenly increasing the rate, and vice versa. Or, I can slowly increase the rate, and see if I can achieve a gradual change in scale. Finally, I will be able to see, indirectly, how penetration rate affects the pattern scale.

I am also working on two potentially useful probes of the starch's interior. Learning from the noise inherent in the thermal probe as initially constructed, I have rebuilt the probe using coaxial cables. I have calibrated the thermistors of this probe, but have not yet been able to test it in starch. An alternative, interesting probe is still

tentative, but promising. A pair of bare tipped wires immersed in moist starch has a resistance of about 200 000 Ω/cm. During an experiment with such wires immersed in a starch slurry, it was observed that, as the drying front passed the wire tips, the resistance increases by over 2 orders of magnitude. By having such wires placed at different depths the front width and velocity may be measurable.

Research jointing is now at the point now where comparison between experimental and theoretical results would be useful. To this end, I have identified four theoretical models which should be investigated further. The first is based on models by Smalley [42], and Budkewitsch and Robin [3], where voronoi tessellations are used to model and predict the behavior of a maturing colonnade. I have implemented Budkewitsch and Robin's VOPOUNCE (**Vo**ronoi **po**lygons **nu**cleated on the **ce**ntroid) algorithm in Matlab (see Appendix B), but have not yet characterized it using the statistics familiar to my experiments. The next interesting model is be atomistic, based on balls and springs, and would be written similarly to those of Hayakawa [12], or Jagla and Rojo [17]. I have played with a 1D simulation written in Microsoft Visual Basic, but have not yet pursued this model further. The third model is a stress-strain investigation of the influence of existing cracks on the evolution of a 3D crack pattern. Something like this has been done in 2D [17], and in a octagon-quadrangle 3D pattern [38]. The final model is a continuum model based on diffusive cooling of basalt [10]. This model makes a number of predictions which can be adapted to the patterns grown in starch.

I would also like to extend this work to other media showing columnar jointing. The most interesting possibilities for this are experiments with quenched glass. Other possible lab friendly materials may include clays and mud, other types of starch, or colloid laced ice. Even simply compiling the conditions under where these materials form columns may lead to an understanding of this phenomena. These experiments would be vital to an attempt to explain the physical origin of the crack pattern scale.

Finally, with the results of my cornstarch experiments, a reappraisal of the basaltic colonnades may be useful. This would best be done by field work, which could be accomplished as a direct continuation of this research.

In general, a basalt flow cools from both top and bottom. As described in the introduction, discontinuities arise when these fronts meet, between colonnades and entablatures, and between colonnades of differing scales. This last type of transition

may correspond with the sharp transition of pattern scale seen in starch. If so, there should be indications of this left in the rock.

Cooling of basalt may occur by heat diffusion, or convection of water involving rainfall and flooding [23, 10, 7]. All these mechanisms are highly variable: a diffusing front slows down; rainfall is seasonal; and flooding is by its very nature, intermittent. However, a basalt colonnade maintains a regular pattern and scale, despite the resulting variations in the crack front width and velocity. This is one of the mysteries of this phenomena. However, it may have a simple explanation: the resistance to scale changes seen in starch must also act in basalt. This would mean that short term (which, given the slow cooling rate of basalt would include seasonal variation) variations would not produce a significant change in column scale, unless they are substantial enough to produce a catastrophic change.

This stability may be field tested by observing the striae of a colonnade, the width of which are representative of the crack front width [37]. Statistically significant variation of the average striae width within a colonnade would support the theory of a hysteretic pattern. A smooth variation across a colonnade boundary would also indicate the same thing.

Other measurements in basalt would also be useful. An investigation of the relationship of crack width to length in entablatures may help to understand what creates some fractures as columns, while some as irregularly cracked rock. A reevaluation of a flow cross-section with attention paid to neighbors (rather than edges), and the transience of X-joints would further test the equivalence of the patterns in starch and basalt. A close look at discontinuities in scale could yield interesting results. Further, the growth of the pattern scale which has been reported near flow surfaces has never been studied in detail. Measurements along the edge of a coarsening flow could fill in this gap in our knowledge, and help understand the ordering process in basalt. Finally, a reappraisal, using modern techniques, of the relationship between column size and cooling rate could eventually lead to the use of columnar joints as a diagnostic tool in the field.

Chapter 4

Conclusion

This study has been a preliminary investigation into the patterns formed in desiccating corn starch. As such, the focus of the work is rather new, even considering that it ties into centuries of scholarship. These were almost entirely simple experiments, with the benefit that, if they didn't work, there was little effort lost. However, many did work. As I started to experiment, I had little idea of what to expect, and what I did expect was often misconceived. For example, the discovery of sudden jumps in column scale started as an attempting to repeat an experiment of Müller [28], where he describes a transition from colonnade to entablature. And I certainly did not expect the revelation that all these crack patterns are topologically hexagonal. Other results, such as the interesting behavior of $CoCl_2$ and $CuSO_4$, were the result of experiments designed for a totally different purpose.

Overall, the course of this work has turned out well, and has identified several fruitful areas meriting further research, in both starch, and new media. The quantitative description of a growing starch colonnade has succeeded in describing a quasihexangonal crack pattern's statistics in all three dimensions, for the first time. And, in doing so it has shown results that have a direct bearing on existing theories of crack formation. The results, including the hypothesis of a hysteretic pattern, need to be further tested, providing opportunities for a continued project.

As I have researched columnar jointing I have been impressed by two things. First, that this is a remarkably general phenomenon, producing the same pattern on a million different scales in a surprising range of materials. Secondly, that not much

effort is required to force a crack pattern into a colonnade. It seems to me that the driving mechanism of columnar jointing must be simple, if not yet fully understood.

Appendices

Appendix A: Labview code

The following three programs, written in Labview 6.1 form the core of the computer controlled feedback experiment.

scale controls.vi is the basic interface between scale and computer, and allows the settings of the scale to be modified by sending the appropriate ASCII sequence.

weigh.vi will, when run, extract the current weight from a bit stream sent by the scale, format it into an decimal, and present it as output.

Evaporation control v2.vi is the control sequence which monitors the weight of a starch sample, and adapts the duty cycle of overhead heat lamps and fans to maintain a constant drying rate. It is designed to be easily adaptable to other experiments.

Appendix B: Matlab Code

What follows are the codes written to produce a voronoi tessellation, and to modify it according to the model of Budkewitsch and Robin [3].

vm3.m is the main program, while vor1.m has been modified from Matlab's native Voronoi command.

Connector Pane

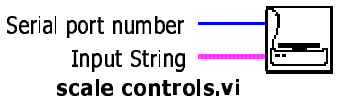

Front Panel

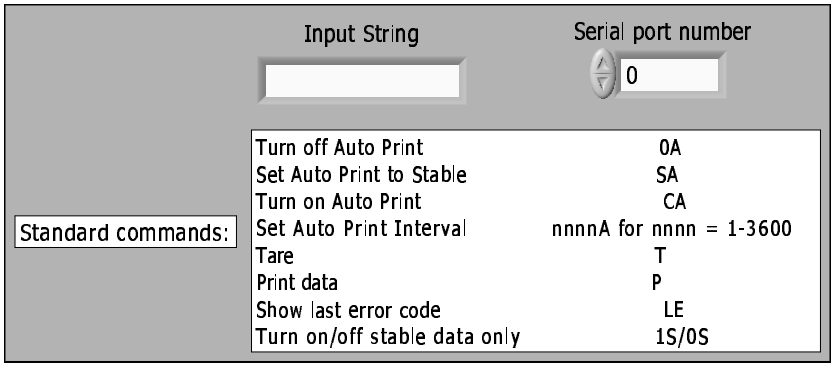

Block Diagram

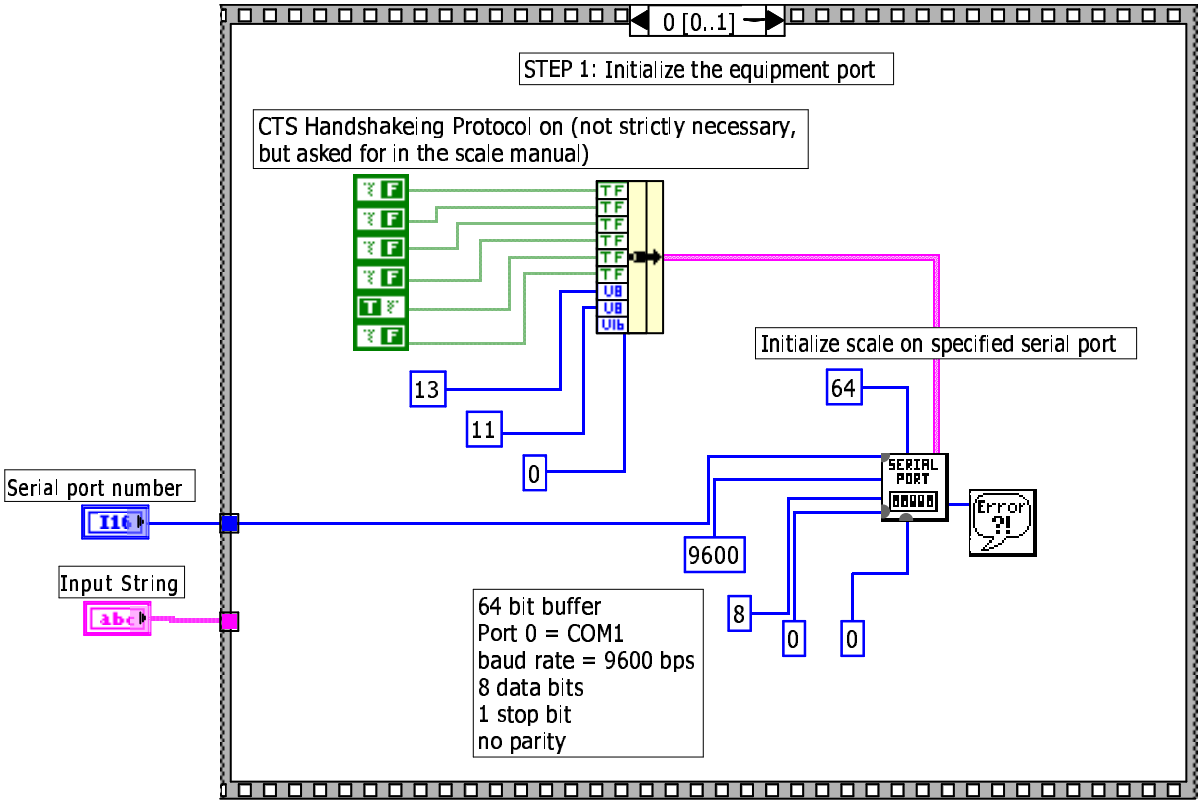

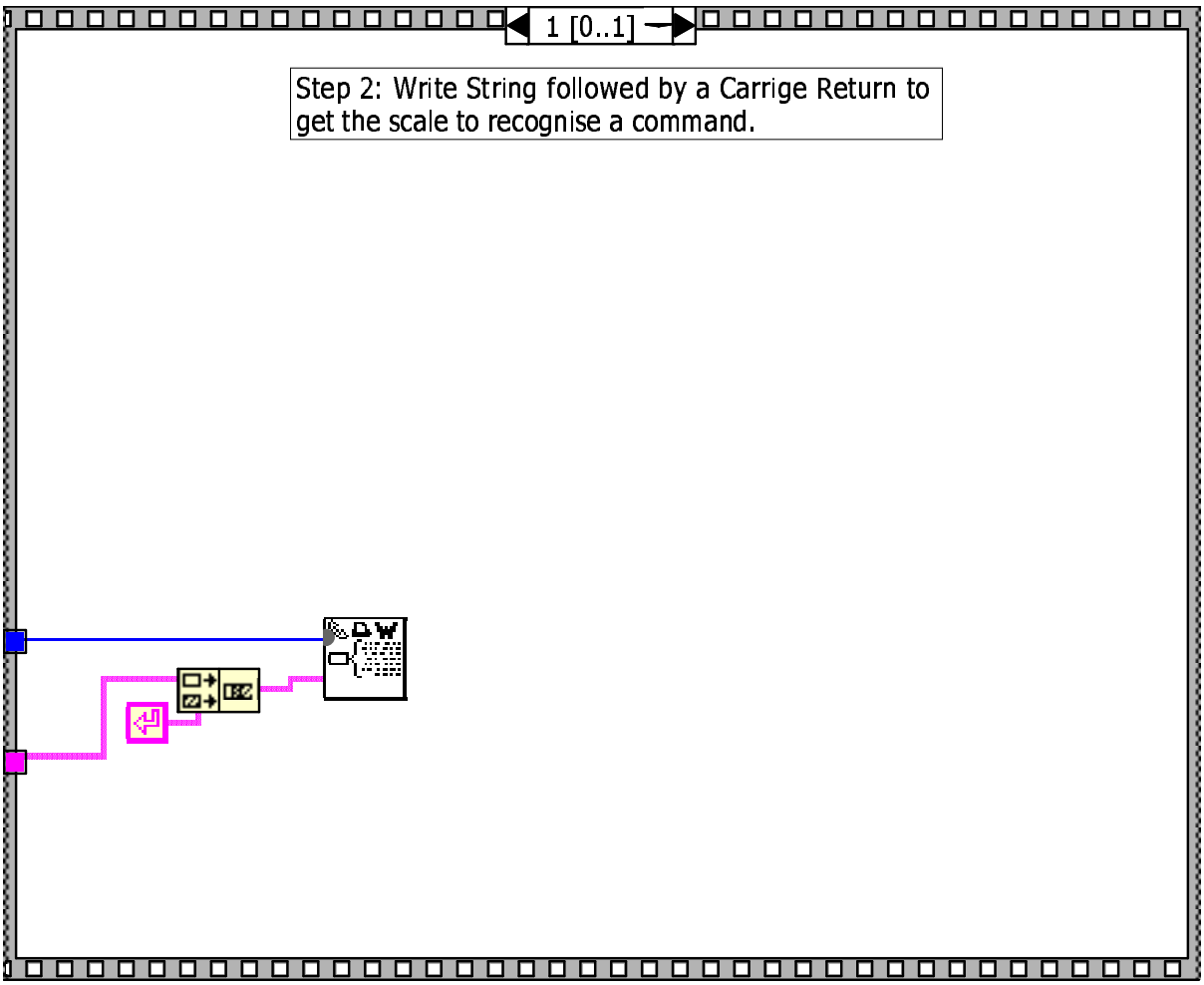
1 [0..1]
Step 2: Write String followed by a Carrige Return to get the scale to recognise a command.

Connector Pane

Front Panel

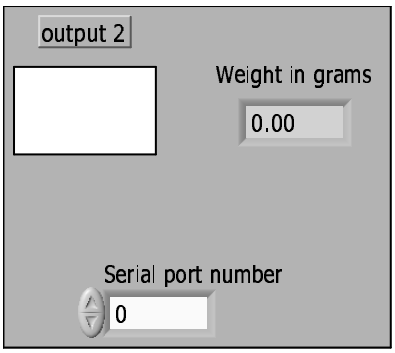

Block Diagram

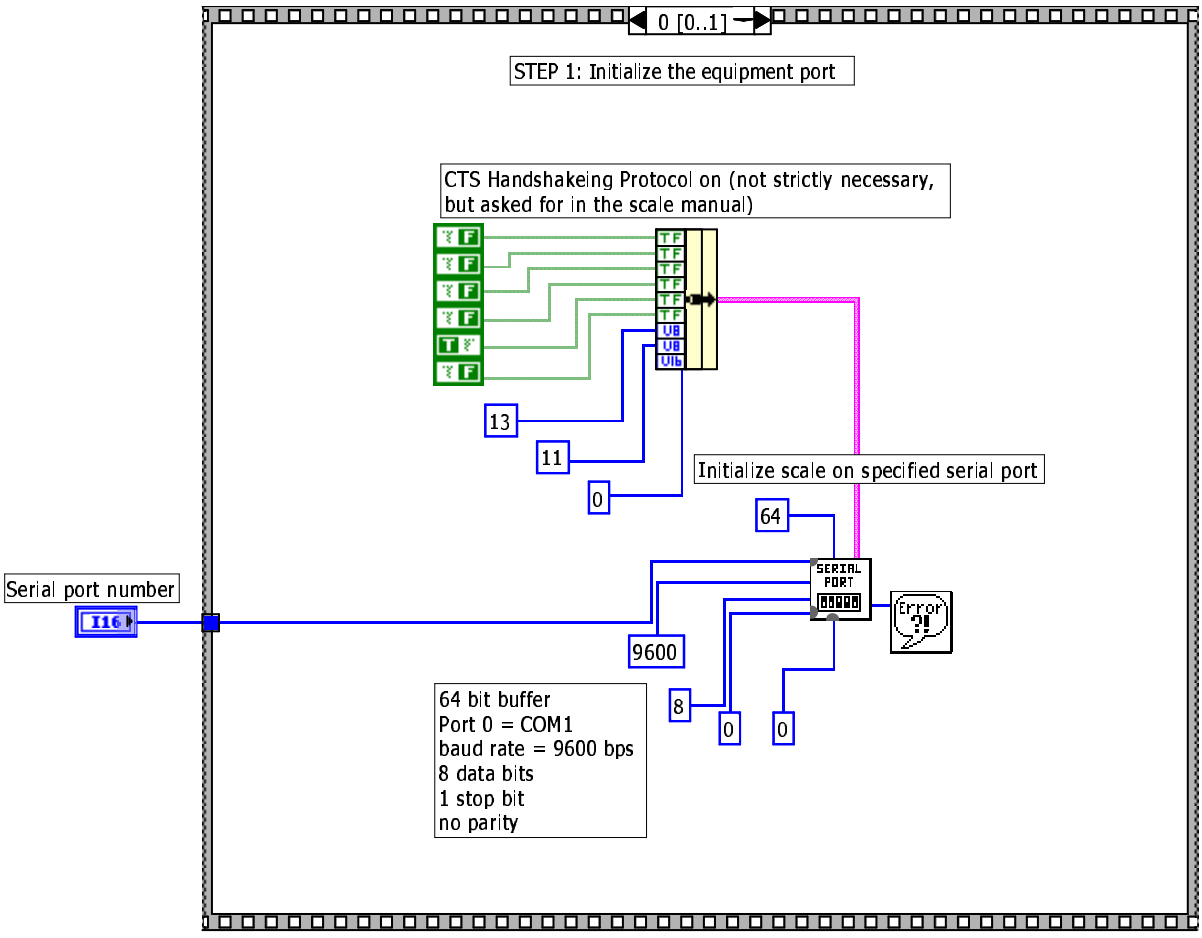

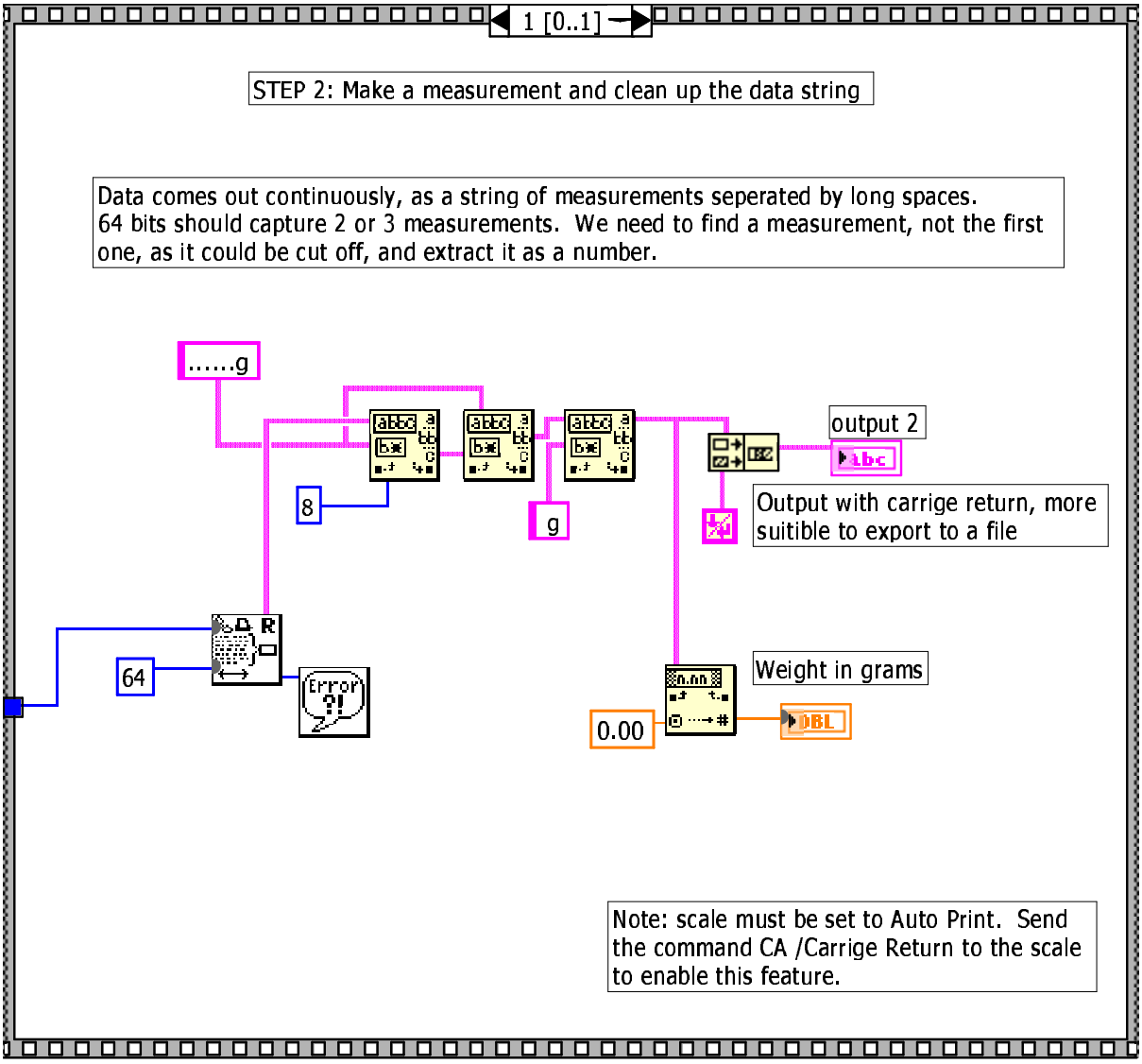
1 [0..1]
STEP 2: Make a measurement and clean up the data string
Data comes out continuously, as a string of measurements seperated by long spaces.
64 bits should capture 2 or 3 measurements. We need to find a measurement, not the first one, as it could be cut off, and extract it as a number.
.....g
8
g
64
Error
output 2
Output with carrige return, more suitible to export to a file
0.00
Weight in grams
Note: scale must be set to Auto Print. Send the command CA /Carrige Return to the scale to enable this feature.

Connector Pane

Evaporation control v2.vi

Front Panel

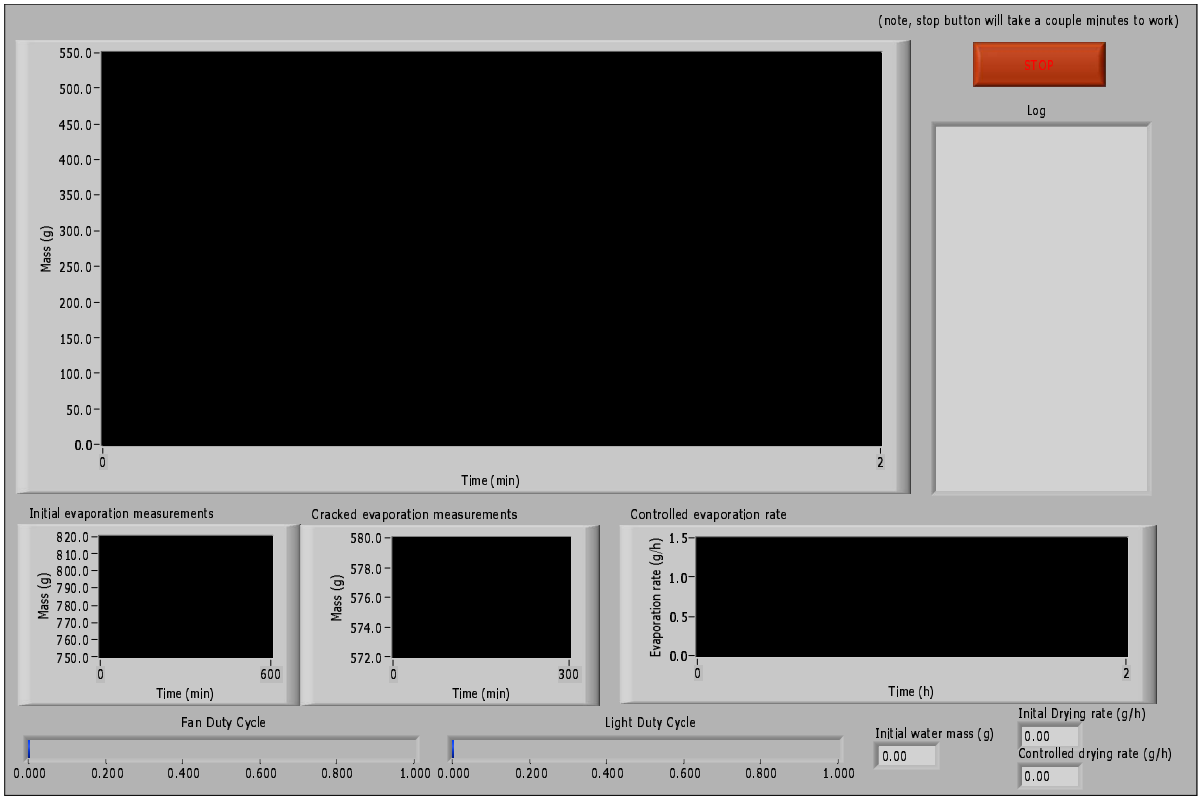

Block Diagram

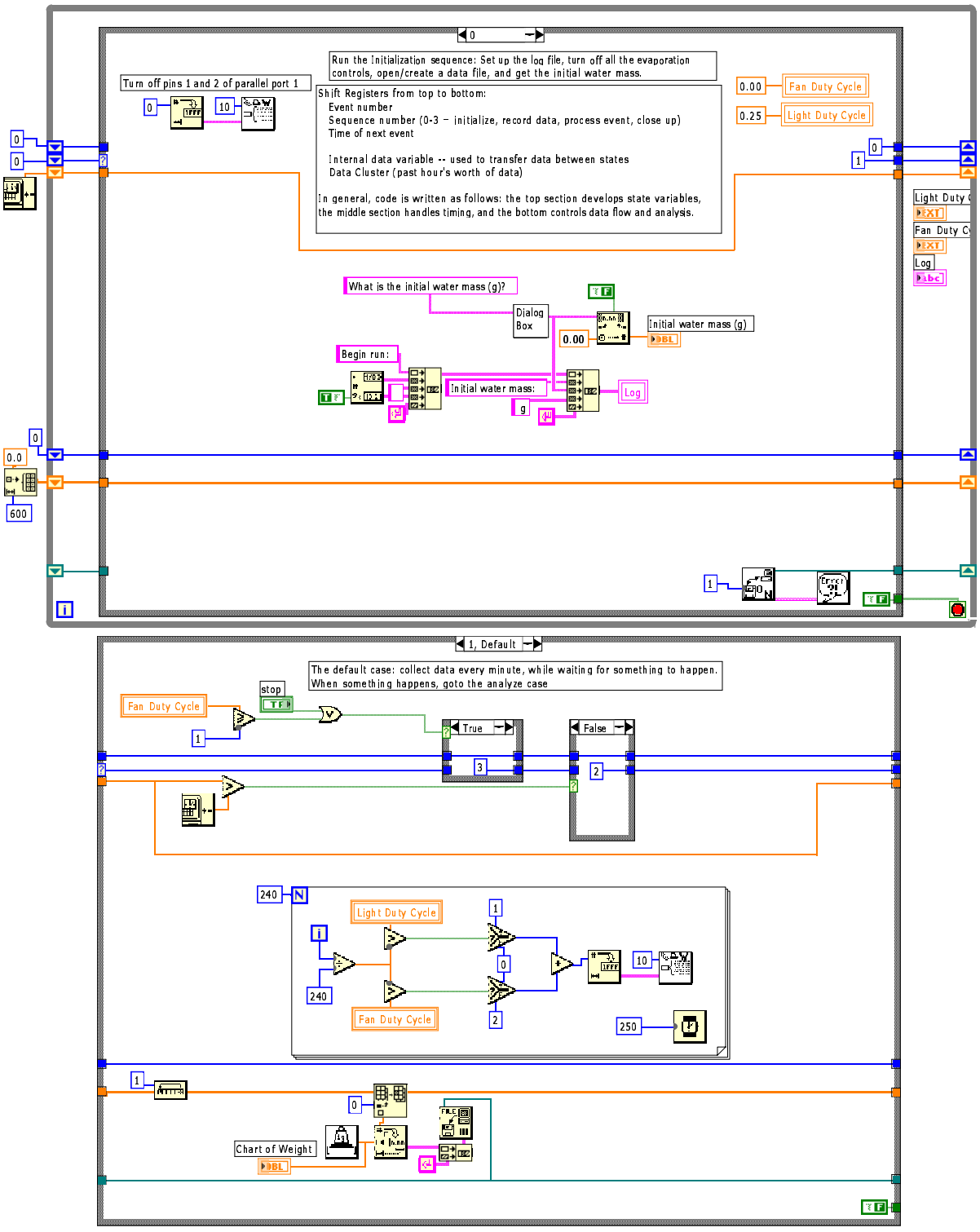

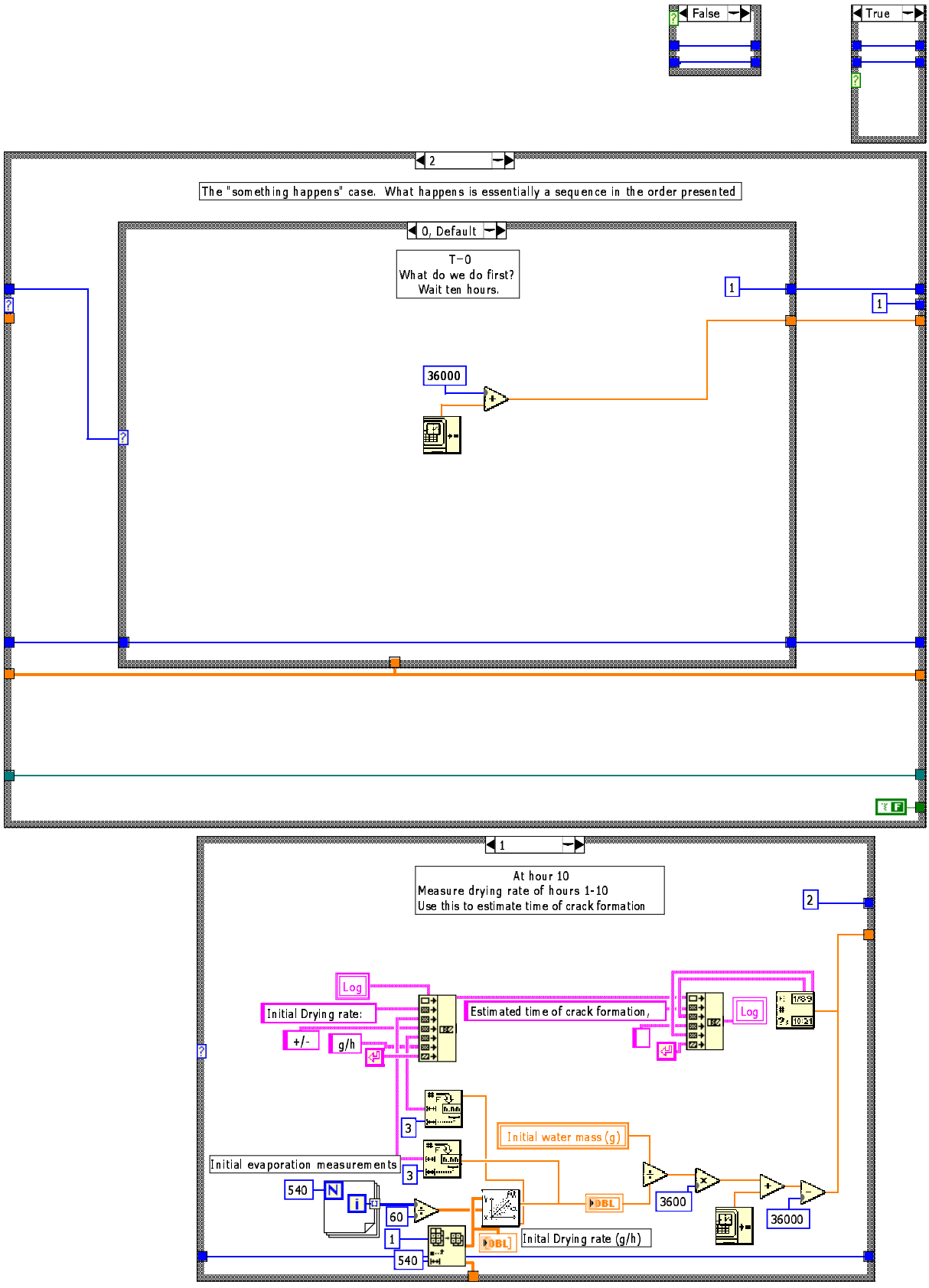
False
True
2
The "something happens" case. What happens is essentially a sequence in the order presented
0, Default
T=0
What do we do first?
Wait ten hours.
1
1
36000
1
At hour 10
Measure drying rate of hours 1-10
Use this to estimate time of crack formation
2
Log
Initial Drying rate:
+/-
g/h
Estimated time of crack formation,
Log
3
Initial water mass (g)
Initial evaporation measurements
3
540
60
1
540
DBL
Inital Drying rate (g/h)
3600
36000

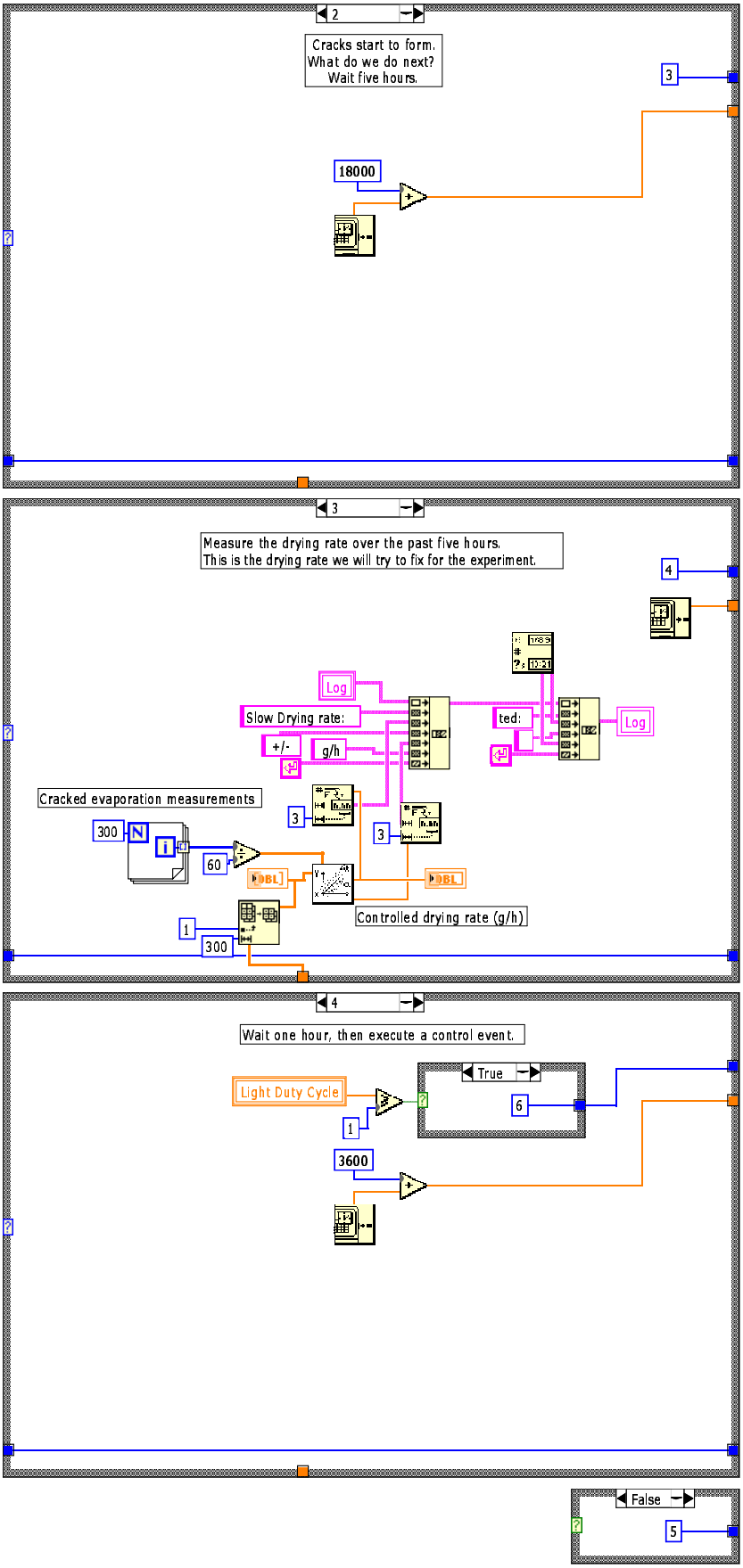
2
Cracks start to form.
What do we do next?
Wait five hours.
3
18000
3
Measure the drying rate over the past five hours.
This is the drying rate we will try to fix for the experiment.
4
Log
Slow Drying rate:
+/-
g/h
ted:
Log
Cracked evaporation measurements
300
60
3
3
DBL
DBL
1
300
Controlled drying rate (g/h)
4
Wait one hour, then execute a control event.
Light Duty Cycle
1
True
6
3600
False
5

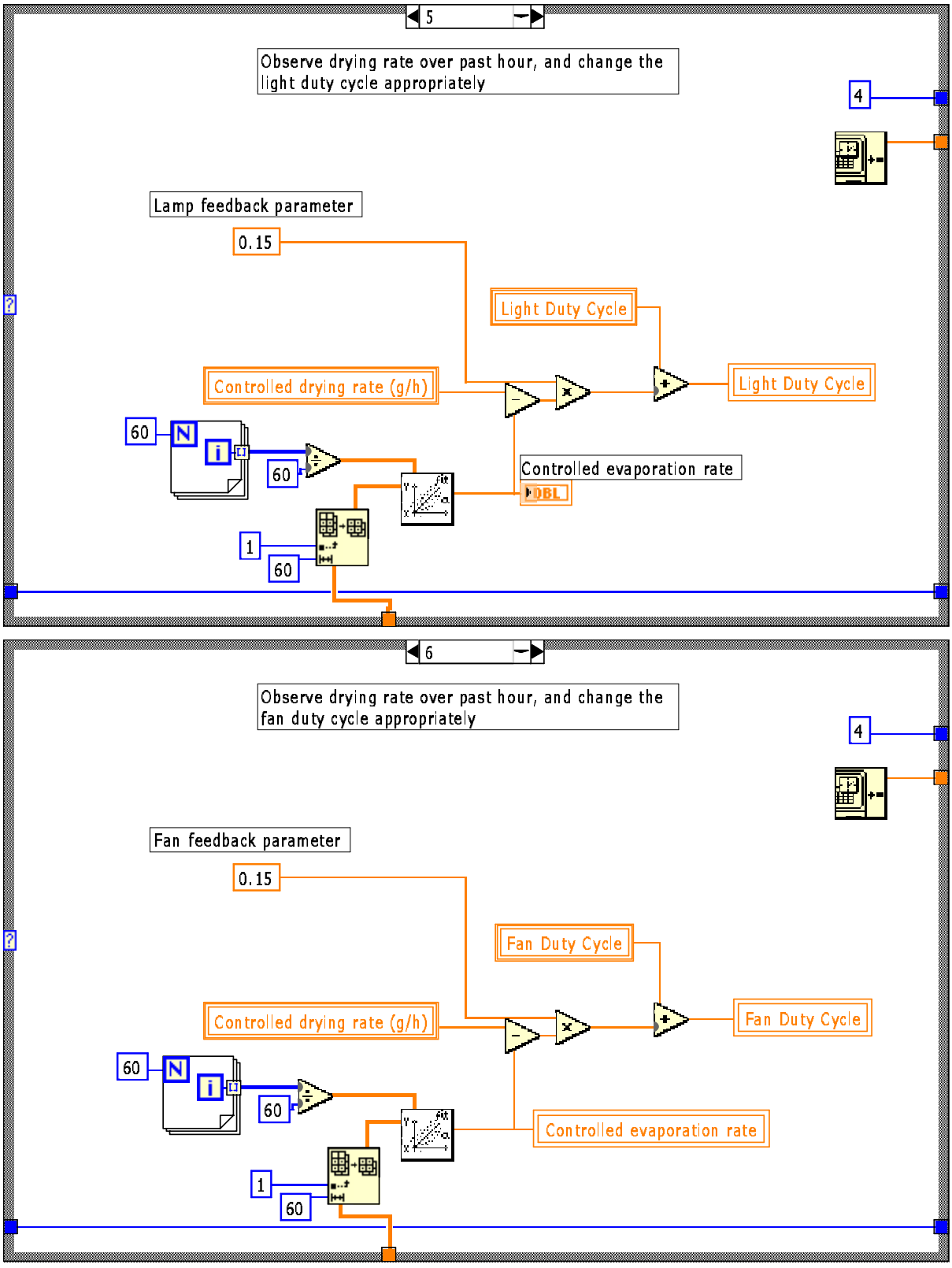
5
Observe drying rate over past hour, and change the light duty cycle appropriately
4
Lamp feedback parameter
0.15
Light Duty Cycle
Controlled drying rate (g/h)
Light Duty Cycle
60
60
Controlled evaporation rate
DBL
1
60
6
Observe drying rate over past hour, and change the fan duty cycle appropriately
4
Fan feedback parameter
0.15
Fan Duty Cycle
Controlled drying rate (g/h)
Fan Duty Cycle
60
60
Controlled evaporation rate
1
60

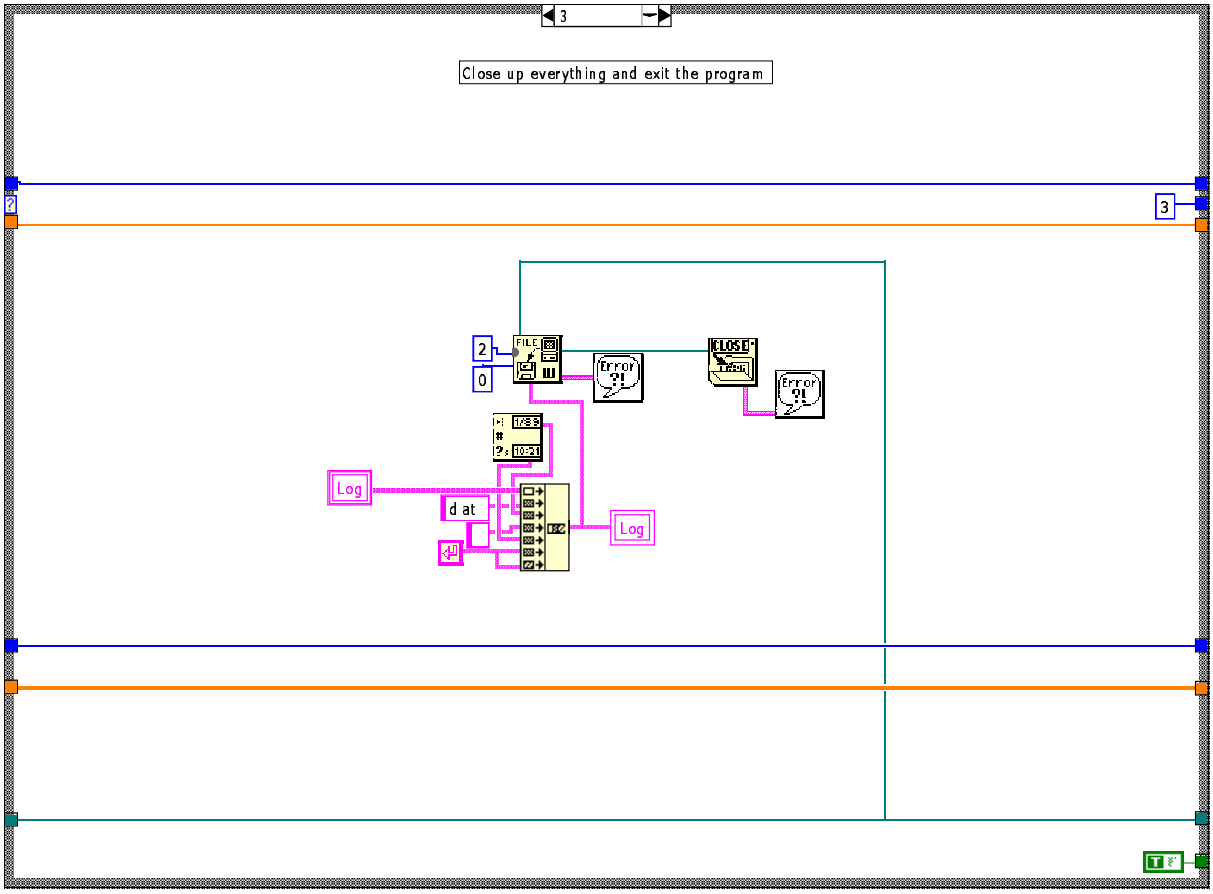
3
Close up everything and exit the program
3
2
0
FILE
Error
CLOSE
Error
Log
d at
Log

```
function twiddle = vm1(n,r1,iter_max,ntimes)

% A program to impliment the Budkewitsch-Robin theory of quasihexagonal crack formation.
% Input parameters         n = number of points along each spacial axis.
%                          r1 = radius of circles used during random close packing.
%                          iter_max = number of iterations used in placing random points.
%                          ntimes = number of iterations of voronoi/centroid updating.

% Step 1: Construct a set of randomly close packed points(circles) on the lattice.
%           Periodic boundary conditions are used.

tic;

testposit=[0,0];
clevel = zeros(n);
testmask = zeros(n);
pointcollectionx = 0;
pointcollectiony = 0;
pointnumber = 0;

figtag1 = 1;
figtag2 = 2;


for k = 1:iter_max
   testposit = [round((n-1)*rand)+1,round((n-1)*rand)+1];
   if testmask(testposit(1),testposit(2)) == 0
      clevel(testposit(1),testposit(2)) = 1;
      pointnumber = pointnumber + 1;
      pointcollectionx(pointnumber) = testposit(1);
      pointcollectiony(pointnumber) = testposit(2);
      for xpos = max([testposit(1)-r1-2,1]):min([testposit(1)+r1+2,n])
         for ypos = max([testposit(2)-r1-2,1]):min([testposit(2)+r1+2,n])
            if sqrt(min([(xpos-testposit(1))^2,(n-xpos+testposit(1))^2])+min([(ypos-
testposit(2))^2,(n-ypos+testposit(2))^2])) <= r1
               testmask(xpos,ypos) = 1;
            end
         end
      end
   end
end
figure(figtag1);
voronoi(pointcollectionx,pointcollectiony);
drawnow;

%  Step 2: Calculate the centroids of the Vornoi polygons for each point.

for z = 1:ntimes

periodicextensionx = [pointcollectionx,pointcollectionx-
n,pointcollectionx,pointcollectionx+n,pointcollectionx-
n,pointcollectionx+n,pointcollectionx-n,pointcollectionx,pointcollectionx+n];
periodicextensiony =
[pointcollectiony,pointcollectiony+n,pointcollectiony+n,pointcollectiony+n,pointcollection
y,pointcollectiony,pointcollectiony-n,pointcollectiony-n,pointcollectiony-n];

for pointnumber = 1:length(pointcollectionx)
   [vx,vy] = vor1(periodicextensionx,periodicextensiony,pointnumber);
   vx1 = vx(1,1);
   vy1 = vy(1,1);
   vertstate = 1;
   Ind = 1;
   k = length(vx);

% We must rearrange the data from Vor1 (a slightly adapted voronoi code, so that they can
be used
```

```
% with the command 'inpolygon'.  This is a tedious, but necessary chore.

   for vertexnum = 1:k
      xtest = (vx - vx1(vertexnum) == 0);
      xtest(vertstate,Ind) = 0;

      while sum(sum(xtest)) ~= 1
         k = k - 1;
         [C,ers] = max(sum(xtest));
         xtest(:,ers) = 0;
      end

      Ind = find(xtest(1,:)+xtest(2,:));
      [C,Ind2] = max(max(xtest'));
      vertstate = 3 - Ind2;
      vx1(vertexnum+1) = vx(vertstate,Ind);
      vy1(vertexnum+1) = vy(vertstate,Ind);
   end

% Now, we must find the centre of mass, using the smallest matricies we can get away with.

   deltax = round(max(vx1)) - round(min(vx1)) + 2;
   deltay = round(max(vy1)) - round(min(vy1)) + 2;
   cutsize = max(deltax,deltay);
   cutx = vx1 - min(vx1);
   cuty = vy1 - min(vy1);
   gen1 = 0;
   gen1(1:cutsize+1) = 0:cutsize;
   xx = repmat(gen1,cutsize+1,1);
   yy = repmat(gen1',1,cutsize+1);

   mask2 = inpolygon(xx,yy,cutx,cuty);

   pointcollectionx(pointnumber) = min(vx1) + sum(sum(xx.*mask2))/sum(sum(mask2));
   pointcollectiony(pointnumber) = min(vy1) + sum(sum(yy.*mask2))/sum(sum(mask2));
   length(pointcollectionx) - pointnumber;

end;
figure(figtag2);
voronoi(pointcollectionx,pointcollectiony);
drawnow;
figtag2 = figtag2 + 1;

end
toc;
```

```
function [vxx,vy] = vor1(x,y,n)
%VORONOI Voronoi diagram.
%   VORONOI(X,Y) plots the Voronoi diagram for the points X,Y.
%
%   VORONOI(X,Y,TRI) uses the triangulation TRI instead of
%   computing it via DELAUNAY.
%
%   H = VORONOI(...,'LineSpec') plots the diagram with color and linestyle
%   specified and returns handles to the line objects created in H.
%
%   [VX,VY] = VORONOI(...) returns the vertices of the Voronoi
%   edges in VX and VY so that plot(VX,VY,'-',X,Y,'.') creates the
%   Voronoi diagram.
%
%   See also DELAUNAY, TRIMESH, TRISURF, DSEARCH, CONVHULL.

%   Clay M. Thompson 7-15-95
%   Copyright (c) 1984-98 by The MathWorks, Inc.
%   $Revision: 1.7 $  $Date: 1997/11/21 23:46:58 $

%   Modified May, 2003, Lucas Goehring.

tri2 = delaunay(x,y);
tri = 0;
count = 1;

ls = '';
for t = 1:size(tri2)
   if tri2(t,1) == n
      tri(count,1:3) = tri2(t,1:3);
      count = count + 1;
   end
   if tri2(t,2) == n
      tri(count,1:3) = tri2(t,1:3);
      count = count + 1;
   end
   if tri2(t,3) == n
      tri(count,1:3) = tri2(t,1:3);
      count = count + 1;
   end
end

n = prod(size(x));
ntri = size(tri,1);
t = (1:ntri)';
T = sparse(tri,tri(:,[3 1 2]),t(:,ones(1,3)),n,n); % Triangle edge if T(i,j)

E = (T & T').*T; % Voronoi edge if E(i,j)

[i,j,v] = find(triu(E));
[i,j,vv] = find(triu(E'));
c1 = circle(tri(v,:),x,y);
c2 = circle(tri(vv,:),x,y);

vx = [c1(:,1) c2(:,1)].';
vy = [c1(:,2) c2(:,2)].';

if nargout<2
   if isempty(ls),
    clf;
    co = get(gcf,'defaultaxescolororder');
    h = plot(vx,vy,'-','color',co(1,:));
  else
    [l,c,m,msg] = colstyle(ls); error(msg)
    if isempty(m), m = '.'; end
    h = plot(vx,vy,ls,x,y,[c m]);
```

```
  end
  if ~ishold,
    view(2), axis([min(x(:)) max(x(:)) min(y(:)) max(y(:))])
  end
  if nargout==1, vxx = h; end
else
  vxx = vx;
end

function c = circle(tri,x,y)
%CIRCLE Return center and radius for circumcircles
%   C = CIRCLE(TRI,X,Y) returns a N-by-3 vector containing [xcenter(:)
%   ycenter(:) radius(:)] for each triangle in TRI.

% Reference: Watson, p32.
x = x(:); y = y(:);

x1 = x(tri(:,1)); x2 = x(tri(:,2)); x3 = x(tri(:,3));
y1 = y(tri(:,1)); y2 = y(tri(:,2)); y3 = y(tri(:,3));

% Set equation for center of each circumcircle:
%    [a11 a12;a21 a22]*[x;y] = [b1;b2] * 0.5;

a11 = x2-x1; a12 = y2-y1;
a21 = x3-x1; a22 = y3-y1;

b1 = a11 .* (x2+x1) + a12 .* (y2+y1);
b2 = a21 .* (x3+x1) + a22 .* (y3+y1);

% Solve the 2-by-2 equation explicitly
idet = a11.*a22 - a21.*a12;

% Add small random displacement to points that are either the same
% or on a line.
d = find(idet == 0);
if ~isempty(d), % Add small random displacement to points
  delta = sqrt(eps);
  x1(d) = x1(d) + delta*(rand(size(d))-0.5);
  x2(d) = x2(d) + delta*(rand(size(d))-0.5);
  x3(d) = x3(d) + delta*(rand(size(d))-0.5);
  y1(d) = y1(d) + delta*(rand(size(d))-0.5);
  y2(d) = y2(d) + delta*(rand(size(d))-0.5);
  y3(d) = y3(d) + delta*(rand(size(d))-0.5);
  a11 = x2-x1; a12 = y2-y1;
  a21 = x3-x1; a22 = y3-y1;
  b1 = a11 .* (x2+x1) + a12 .* (y2+y1);
  b2 = a21 .* (x3+x1) + a22 .* (y3+y1);
  idet = a11.*a22 - a21.*a12;
end

idet = 0.5 ./ idet;

xcenter = ( a22.*b1 - a12.*b2) .* idet;
ycenter = (-a21.*b1 + a11.*b2) .* idet;

radius = (x1-xcenter).^2 + (y1-ycenter).^2;

c = [xcenter ycenter radius];
```

Bibliography

[1] Atilla Aydin and James M. DeGraff, *Evolution of polygonal fracture patterns in lava flows*, Science **239** (1988), 471–476.

[2] Philip Ball, *The self-made tapestry: pattern formation in nature*, Oxford University Press, Oxford, UK, 1999.

[3] Paul Budkewitsch and Pierre-Yves Robin, *Modelling the evolution of columnar joints*, J. Volcanol. Geotherm. Res. **59** (1994), 219–239.

[4] Emanuel Mendez da Costa, *An account of some productions of nature in Scotland resembling the Giants-Causeway in Ireland*, Phil. Trans. R. Soc. Lond. **52** (1761), 103–104.

[5] Ancelem Boèce de Boodt, *Gemmarum et Lapidum Historia*, Lugduni Batovorum, Ex Officina J. Maire, 1647.

[6] James M. DeGraff and Atilla Aydin, *Surface morphology of columnar joints and its significance to mechanics and direction of joint growth*, Geol. Soc. Am. **99** (1987), 605–617.

[7] James M. DeGraff, Philip E. Long, and Atilla Aydin, *Use of joint-growth directions and rock textures to infer thermal regimes during solidification of basaltic lava flows*, J. Volcanol. Geotherm. Res. **38** (1989), 309–324.

[8] Sam Foley and T. Molyneux, *An account of the Giants Caus-Way in the north of Ireland*, Phil. Trans. R. Soc. Lond. **18** (1694), 170–182.

[9] N. H. Gray, J. B. Anderson, J. D. Devine, and J. M. Kwasnik, *Topological properties of random crack networks*, Math. Geol. **8** (1976), 617–626.

[10] Kenneth A. Grossenbacher and Stephen M. McDuffie, *Conductive cooling of lava: columnar joint diameter and stria width as functions of cooling rate and thermal gradient*, J. Volcanol. Geotherm. Res. **69** (1995), 95–103.

[11] Harry C. Hardee, *Solidification in Kilauea Iki Lava Lake*, J. Volcanol. Geotherm. Res. **7** (1980), 211–223.

[12] Y. Hayakawa, *Numerical study of oscillatory crack propegation through a two-dimensional crystal*, Phys. Rev. E **49** (1994), R1804–7.

[13] R. A. Heimlich, *Cylindrical columnar joints in precambrian mafic dykes, Bighorn mountains, Wyoming*, J. of Geol. **77** (1969), 371–374.

[14] D. Hull and B. D. Caddock, *Simulation of prismatic cracking of cooling basalt lava flows by the drying of sol-gels*, J. Mat. Sci. **34** (1999), 5707–5720.

[15] J. P. Iddings, *The columnar structure in the igneous rock on Orange Mountain, New Jersey*, Am. Jour. Sci. **131** (1886), 321–330.

[16] E. A. Jagla, *Stable propegation of an ordered array of cracks during directional drying*, Phys. Rev. E **65** (2002), 046147.

[17] E. A. Jagla and A. G. Rojo, *Sequential fragmentation: The origin of columnar quasihexagonal patterns*, Phys. Rev. E **65** (2002), 026203.

[18] Catherine L. Johnson and David T. Sandwell, *Joints in Venusian lava flows*, J. Geophys. Res. **97** (1992), 13601–13610.

[19] Eric M. Jones, *Apollo 15 Lunar Surface Journal; Hadley Rille*, http://www.hq.nasa.gov/office/pao/History/alsj/a15/a15.rille.html (Last accessed August 25th 2003).

[20] L. H. Kantha, *'Basalt fingers' – origin of columnar joints?*, Geol. Mag. **118** (1981), 251–264.

[21] Kentmannus, *Gesner de Figuris Lapidum.*

[22] A. H. Lachenbruch, *Mechanics of thermal contraction cracks and ice-wedge polygons in permafrost*, Geol. Soc. Am. **Spec. Paper 70** (1962), 69p.

[23] Philip E. Long and Bernard J. Wood, *Structures, textures, and cooling histories of Columbia River basalt flows*, Geol. Soc. Am. Bull. **97** (1986), 1144–1155.

[24] M. Marder, *Cracks take a new turn*, Nature **362** (1993), 295–296.

[25] Fredric M. Menger, Hong Zhang, Kevin L. Caran, Victor A. Seredyuk, and Robert P. Apkarian, *Gemini-induced columnar jointing in vitreous ice. Cryo-HRSEM as a tool for discovering new colloidal morphologies*, J. Am. Chem. Soc. **124** (2002), 1140–1141.

[26] Thomas Molyneux, *Some additional observations on the Giants Causway in Ireland*, Phil. Trans. R. Soc. Lond. **20** (1698), 209–223.

[27] Gerhard Müller, *Experimental simulation of basalt columns*, J. Volcanol. Geotherm. Res. **86** (1998), 93–96.

[28] ———, *Starch columns: Analog model for basalt columns*, J. Geophys. Res. **103** (1998), 15239–15253.

[29] ———, *Experimental simulation of joint morphology*, J. Struct. Geol. **23** (2001), 45–49.

[30] J. P. O'Reilly, *Explanatory notes and discussion on the nature of the prismatic forms of a group of columnar basalts, Giant's Causeway*, Trans. R. Irish Acad. **26** (1879), 641–728.

[31] H. G. Patil, D. I. Deendar, and N. W. Gokhale, *Mini columnar joints in basalts, of Kodali village, Maharashtra*, Current Science **53** (1984), 1089.

[32] Dallas L. Peck and Takeshi Minakami, *The formation of columnar joints in the upper part of Kilauean lava lakes, Hawaii*, Geol. Soc. Am. Bull. **79** (1968), 1151–1166.

[33] Richard Pocock, *A farther account of the Giant's Causeway in the County of Antrim in Ireland*, Phil. Trans. R. Soc. Lond. **48** (1753), 226–237.

[34] Brian R. Pratt, *Septarian concretions: internal cracking caused by synsedimentary earthquakes*, Sedimentology **48** (2001), 189–213.

[35] Sir RBSRS, *Part of a letter from Sir R.B.S.R.S. to Dr. Lister, concerning the Giants Causway in the County of Atrim in Ireland*, Phil. Trans. R. Soc. Lond. **17** (1693), 708–710.

[36] Right Rev. Richard, *An account of a production of nature at Dunbar in Scotland, like that of the Giants-Causeway in Ireland*, Phil. Trans. R. Soc. Lond. **52** (1761), 98–99.

[37] Michael P. Ryan and Charles G. Sammis, *Cyclic fracture mechanisms in cooling basalt*, Geol. Soc. Am. Bull. **89** (1978), 1295–1308.

[38] R. Saliba and E. A. Jagla, *Analysis of columnar joint patterns from 3D stress modeling*, J. Geophys. Res. **to be published** (2003), NA.

[39] J. Sellés-Martínez, *Concretion morphology, classification and genesis*, Earth-Science Rev. **41** (1996), 177–210.

[40] K. V. Seshadri, *Columnar jointing in Mesozoic sandstone of Bhuj series, Kutch Basin, Gujarat, India*, Jour. Geol. Soc. India **49** (1997), 452–453.

[41] Kelly A. Shorlin, John R. de Bruyn, Malcolm Graham, and Stephen W. Morris, *Development and geometry of isotropic and directional shrinkage crack patterns*, Phys. Rev. E. **61** (2000), 6950.

[42] I. J. Smalley, *Contration crack networks in basalt flows*, Geol. Mag. **103** (2066), 110–114.

[43] Wayne Tokaruk, *Personal communication.*

[44] Abraham Trembly, *Remarks on the stones, in the Country of Nassau*, Phil. Trans. R. Soc. Lond. **49** (1756), 581–585.

[45] Hugh Tuffen, Jennie Gilbert, and Dave McGarvie, *Products of an effusive sub-glacial rhyolite eruption: Bláhnúkur, Torfajökull, Iceland*, Bull. Volcanol. **63** (2001), 179–190.

[46] D. Weaire and C. O'Carroll, *A new model for the Giant's Causeway*, Nature **302** (1983), 240–241.

[47] A. Yuse and M. Sano, *Transition between crack patterns in quenched glass plates*, Nature **362** (1993), 329–331.

[48] Lin Zhenquan, Lucas Goehring, and Stephen Morris, *Unpublished data.*